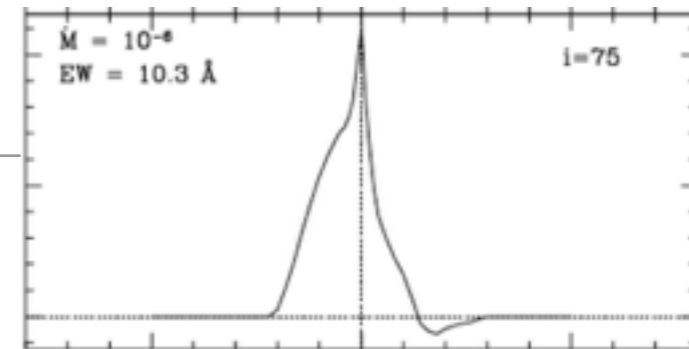
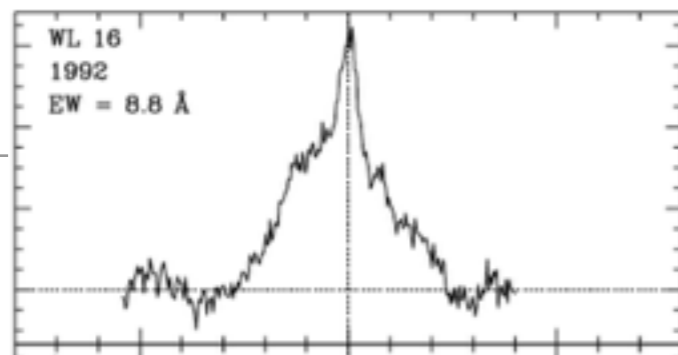


# MAGNETOSPHERIC ACCRETION MODELS FOR THE HYDROGEN EMISSION LINES OF T TAURI STARS

JAMES MUZEROLLE, NURIA CALVET, LEE HARTMANN  
Astrophysical Journal, Volume 492, 743 (1998)

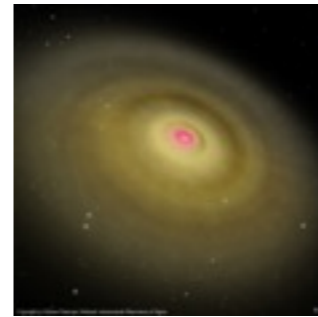


Ábrahám Péter

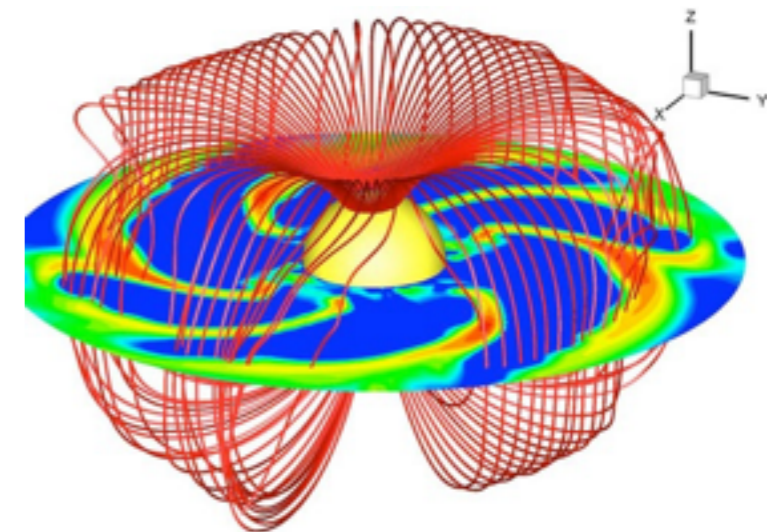
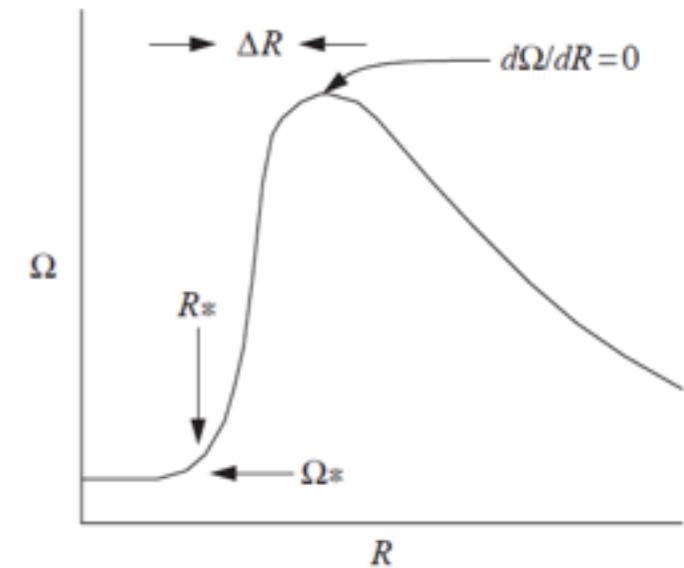
Accretion processes, 2014. november 5.

# Magnetospheric accretion

- ❖ Early models: boundary layer
  - hot material, UV excess
- ❖ Magnetospheric accretion
  - stellar magnetic field truncates the disk
  - gas infall along magnetic lines @ free-fall
- ❖ High latitude accretion shocks
- ❖ X-ray/EUV radiation immediately absorbed, producing UV-optical excess, consistent with observations
- ❖ if accretion occurs in magnetic “columns”, or if the magnetic axis is misaligned with the rotation axis, photometric changes appear



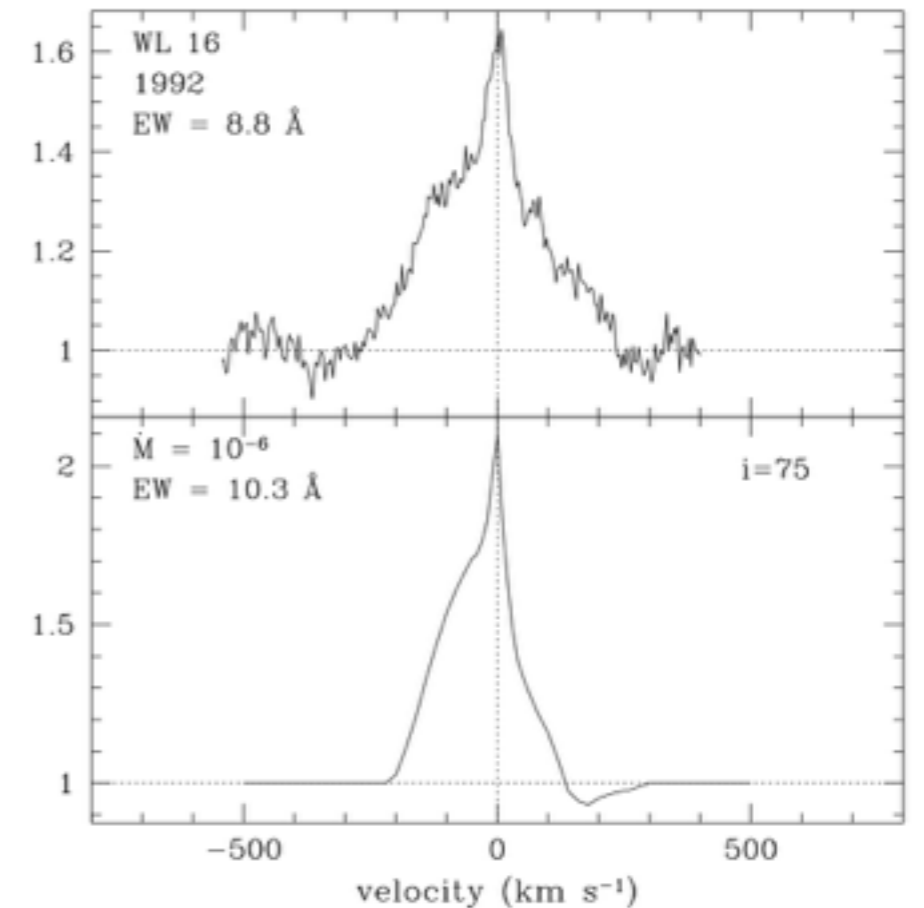
Credit: Subaru Telescope



Credit: M. Romanova

# Magnetospheric accretion: line profiles

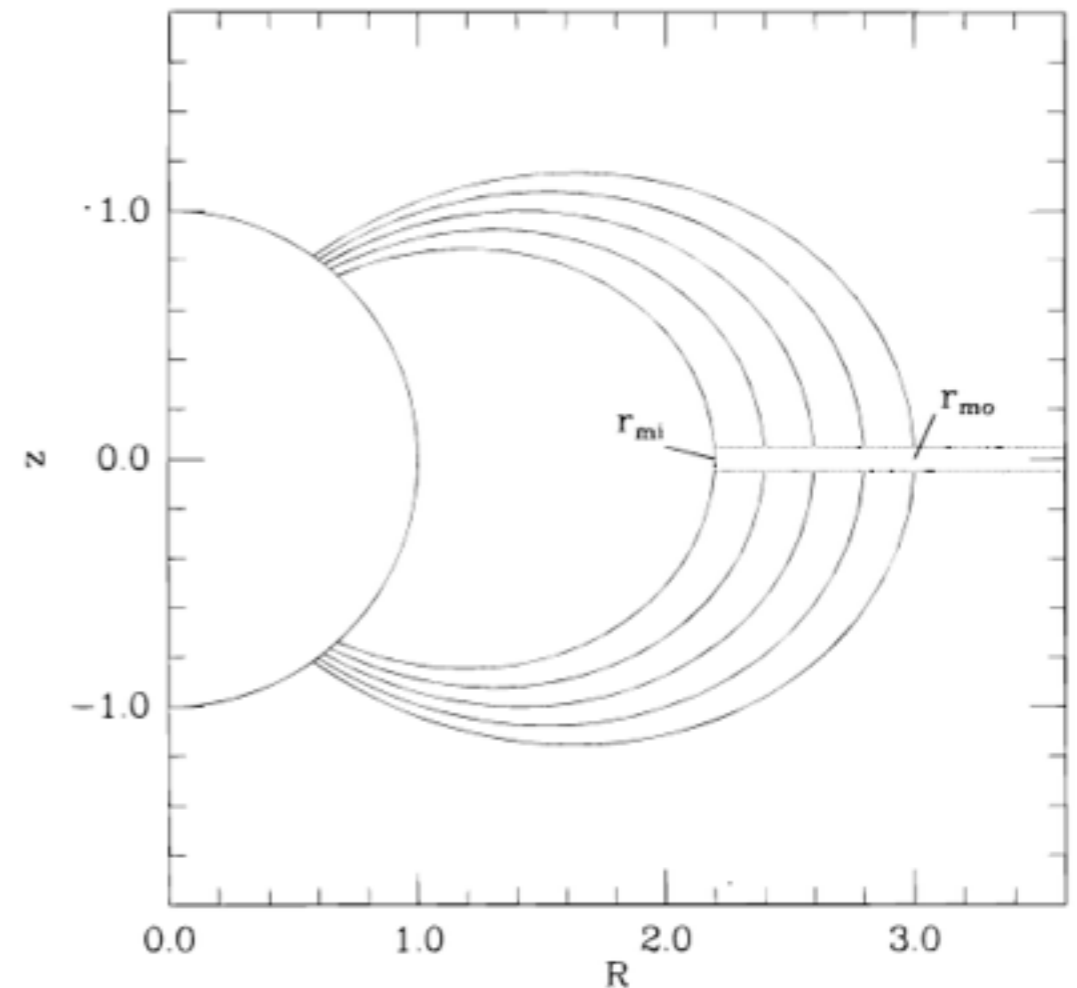
- ❖ Classical T Tauri stars exhibit strong emission lines with large line widths, and sometimes inverse P Cygni profiles
- ❖ H alpha, Br gamma, Ca II, ...
- ❖ redshifted absorption component at several hundred km/s indicates infall from large distances
- ❖ boundary layer cannot produce high enough accretion velocities
- ❖ infall along the magnetic lines will be on ballistic trajectories with free-fall velocity - consistent with observations
- ❖ line radiative transfer of magnetospheric infall can reproduce (unlike stellar winds) line width and central peak
- ❖ redshifted absorption depends on geometry, and is not always seen



Br gamma in WL 16.

# Physical model

- ❖ Hartmann, Hewett, & Calvet (1994) (two-level atoms) model setup
- ❖ Magnetosphere: dipole field, axisymmetric about the rotation axis
- ❖ Disk is opaque and non emitting
- ❖ Stellar mass:  $0.5 M_{\text{sun}}$ , radius:  $2 R_{\text{sun}}$ , photospheric temperature: 4000 K
- ❖ stellar rotation is neglected (slow, compared to the infall velocity, although may be problematic at the bottom of accretion flow)



# Reference cases

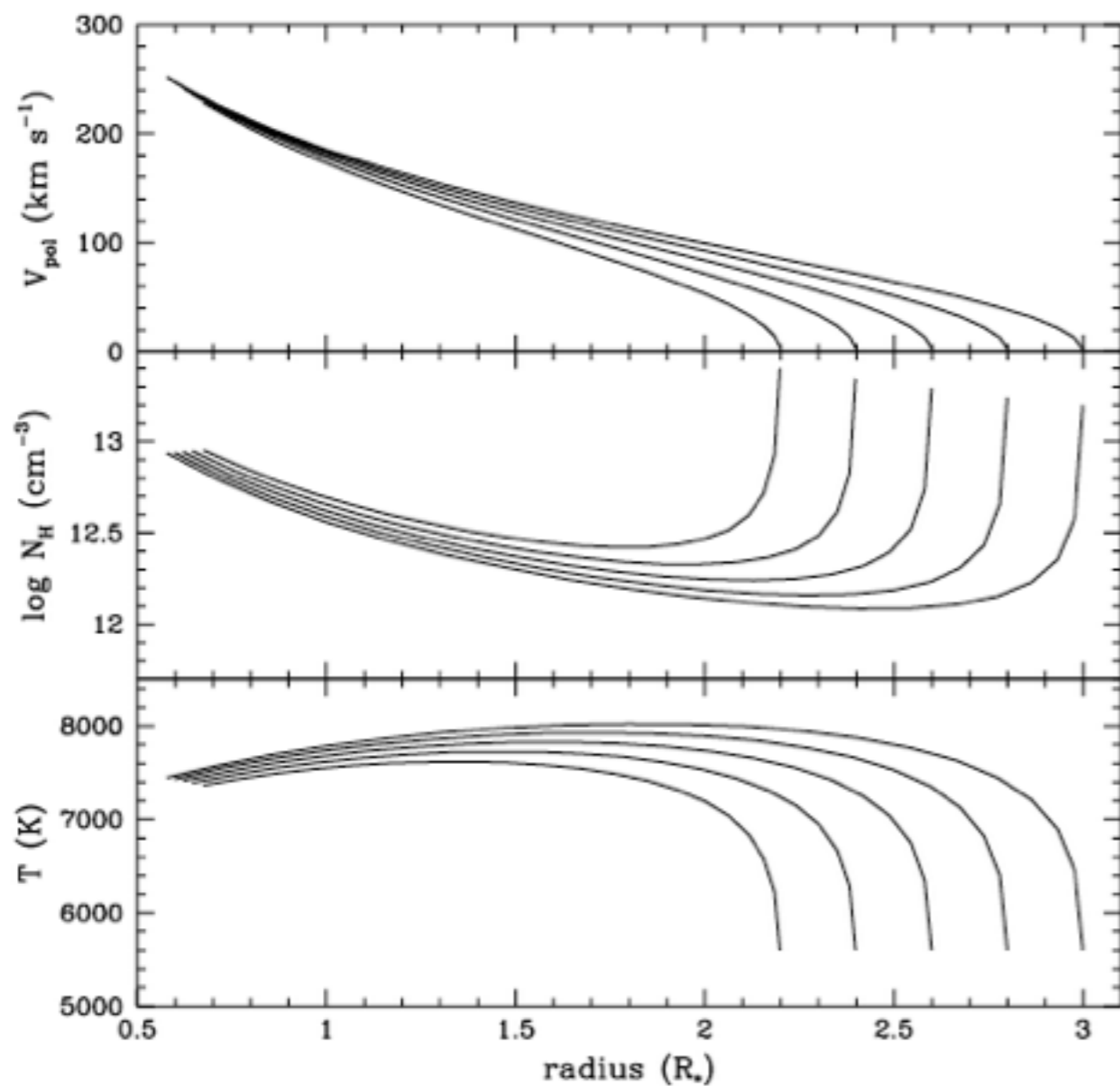


FIG. 2.—Velocity, density, and temperature distributions for a fiducial case:  $\dot{M} = 10^{-7} M_{\odot} \text{ yr}^{-1}$ ,  $T_{\text{max}} = 8000 \text{ K}$ ,  $R_{*} = 2 R_{\odot}$ ,  $M_{*} = 0.5 M_{\odot}$ ,  $r_{\text{mi}} = 2.2 R_{\odot}$ , and  $r_{\text{mo}} = 3 R_{\odot}$ .

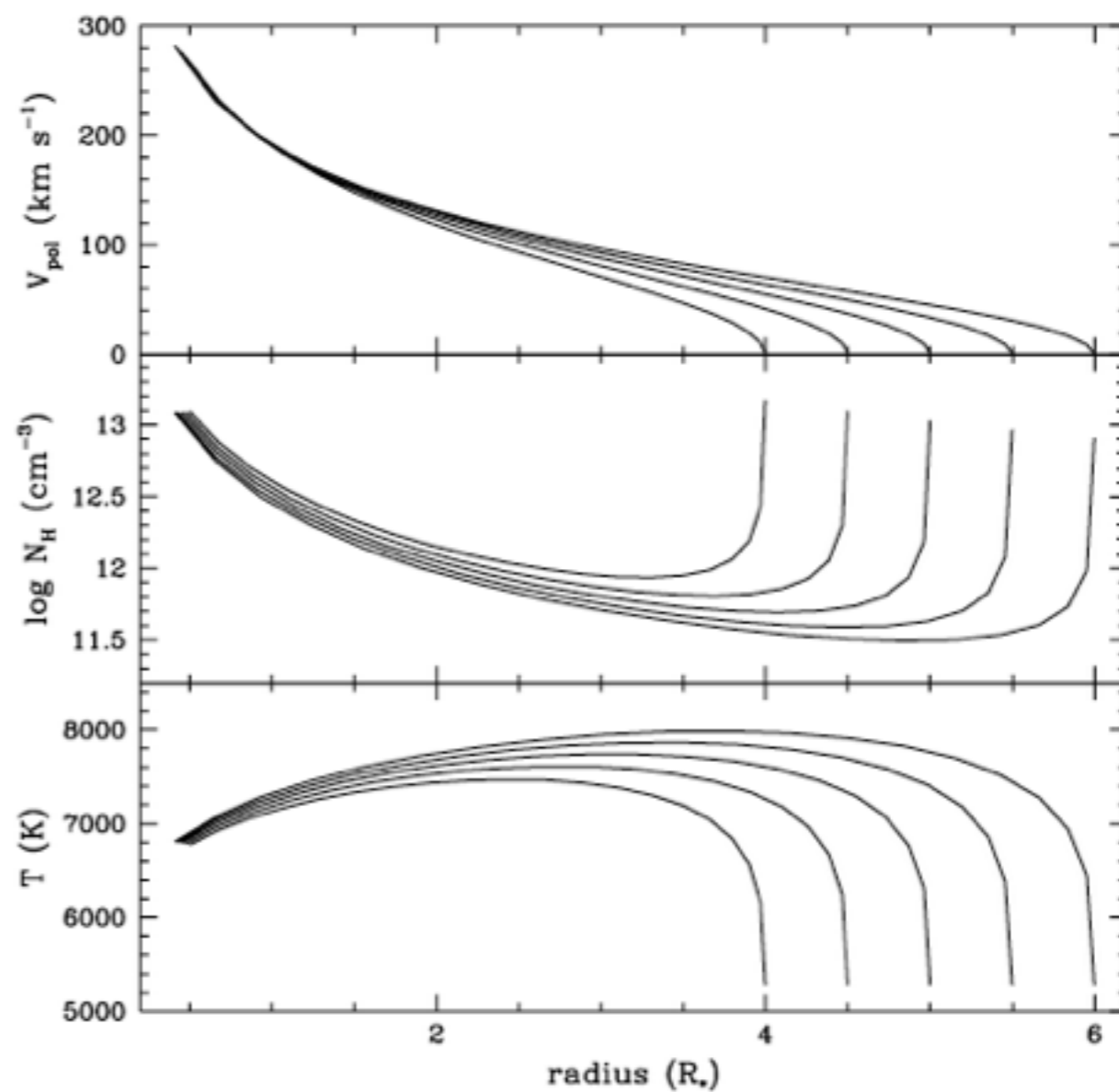


FIG. 3.—Velocity, density, and temperature distributions for a larger magnetosphere:  $\dot{M} = 10^{-7} M_{\odot} \text{ yr}^{-1}$ ,  $T_{\text{max}} = 8000 \text{ K}$ ,  $R_{*} = 2 R_{\odot}$ ,  $M_{*} = 0.5 M_{\odot}$ ,  $r_{\text{mi}} = 4 R_{\odot}$ , and  $r_{\text{mo}} = 6 R_{\odot}$ .

# Radiative transfer

---

- ❖ Extended Sobolev RT method
- ❖ Applicable in the case of large non-monotonic velocity gradient (probably true for the broad T Tau lines, supersonic flows)
- ❖ Line radiative transfer
- ❖ Line optical depths are determined from the line opacities and velocity gradients at each point
- ❖ Line source function (ratio of emission to absorption coefficients):
  - simple 2-level atom approximation:  $S(r) = [1 - \epsilon(r)]\bar{J}(r) + \epsilon(r)B(r)$   
(epsilon(r) is the destruction probability, i.e., the ratio of collisional to total deexcitation rates):
  - multilevel calculations: *cvmulti*

$$S_{ul} = \frac{2hv_{ul}^3}{c^2} \left[ \left( \frac{N_l g_u}{N_u g_l} \right) - 1 \right]^{-1}$$

# Radiative transfer

---

- ❖ Electron density:
- ❖ calculate from the first two ionization stages of all elements up to iron, using the appropriate abundances and assuming LTE
- ❖ The total electron density is the sum of the hydrogen continuum population (protons) plus the total number of ionizations (electrons) from the metals.
- ❖ Iterative process

# Profiles: comparison with the two-level model

- ❖ Shapes are very similar
- ❖ *cvmulti* lines are weaker
- ❖ reason: the presence of multiple upper levels

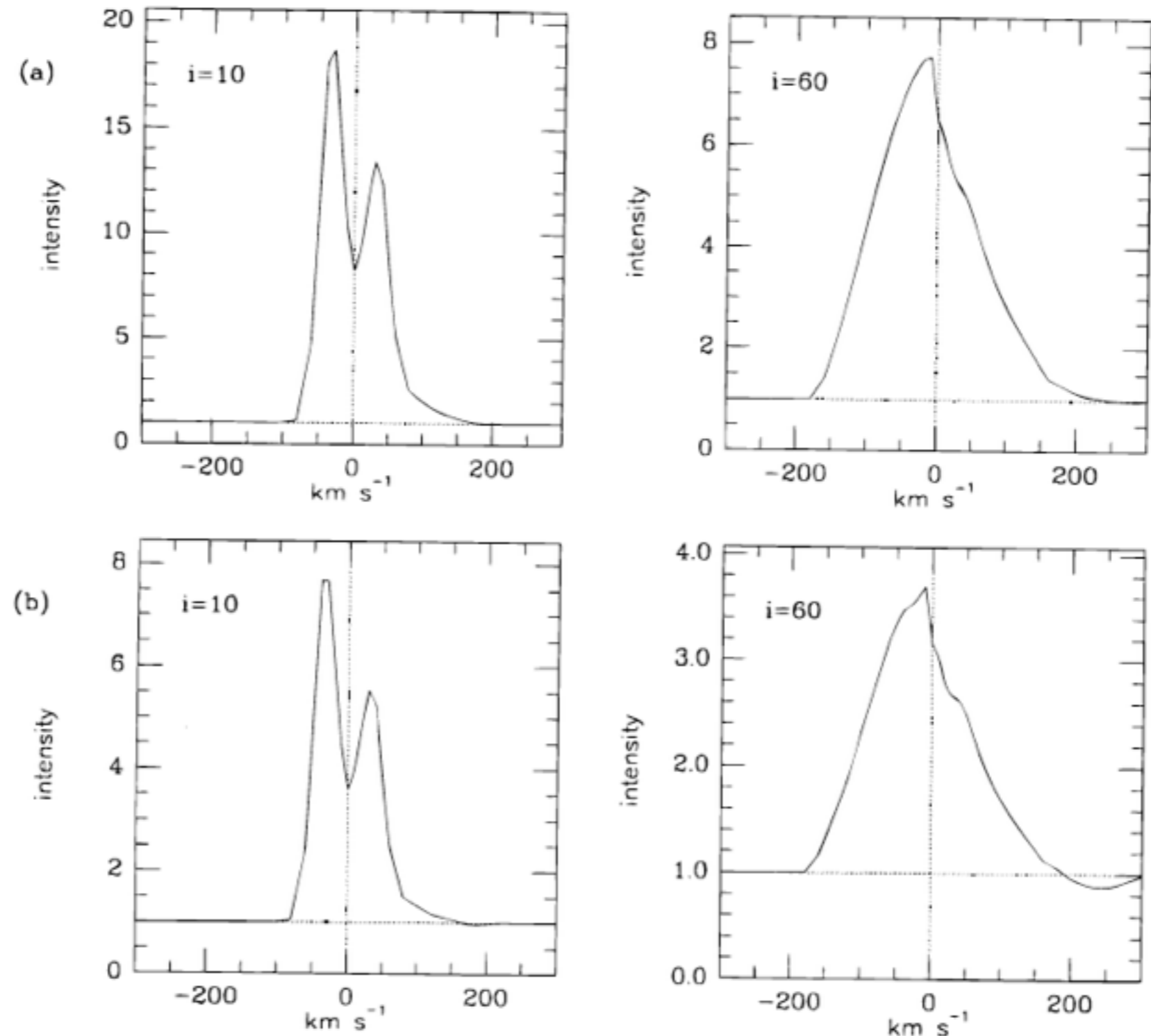
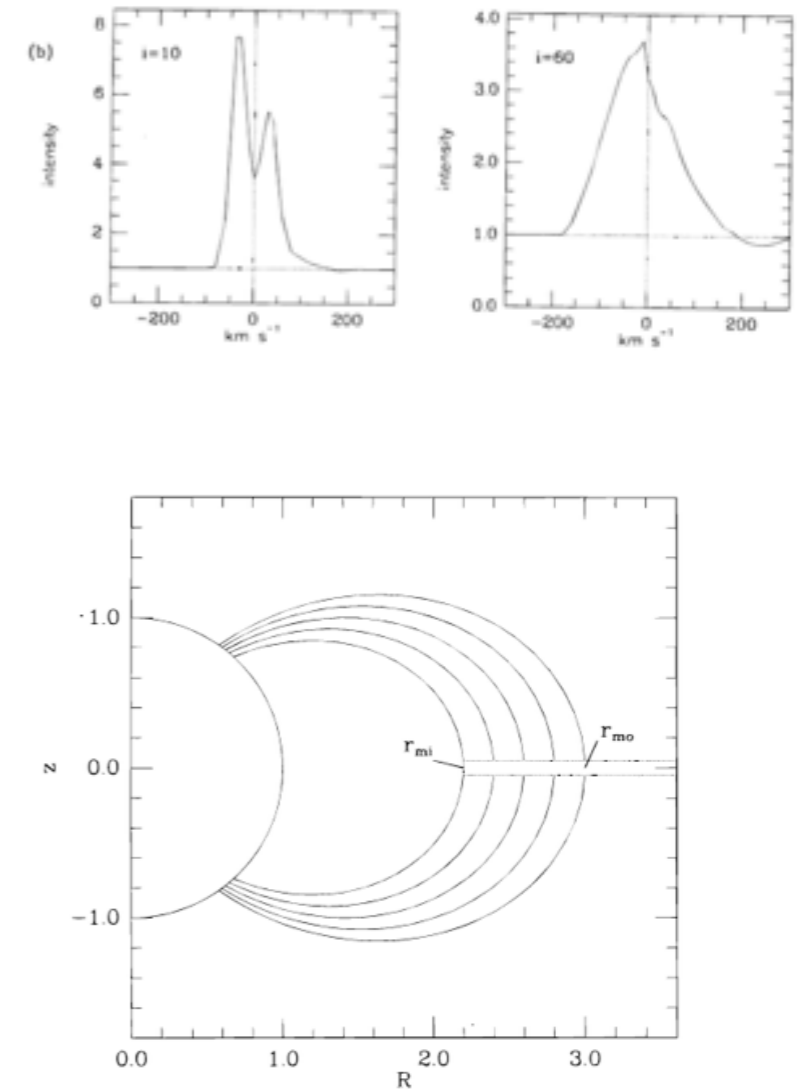


FIG. 4.—Comparison of H $\alpha$  profiles for the case of  $\dot{M} = 10^{-7} M_{\odot} \text{ yr}^{-1}$ ,  $T_{\text{max}} = 7500 \text{ K}$ ,  $R_{*} = 2 R_{\odot}$ ,  $M_{*} = 0.8 M_{\odot}$ ,  $r_{\text{mi}} = 2.2 R_{\odot}$ , and  $r_{\text{mo}} = 3 R_{\odot}$  for (a) HHC results and (b) *cvmulti* results.

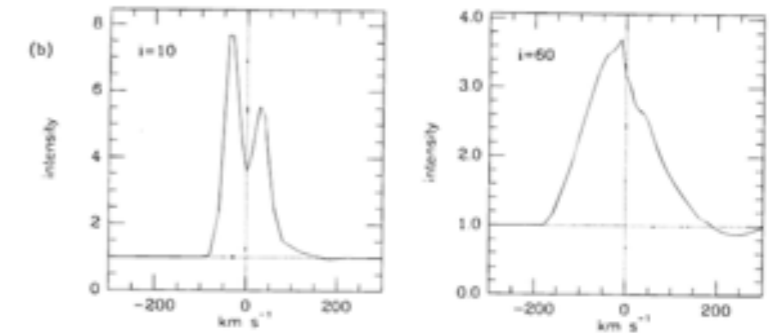
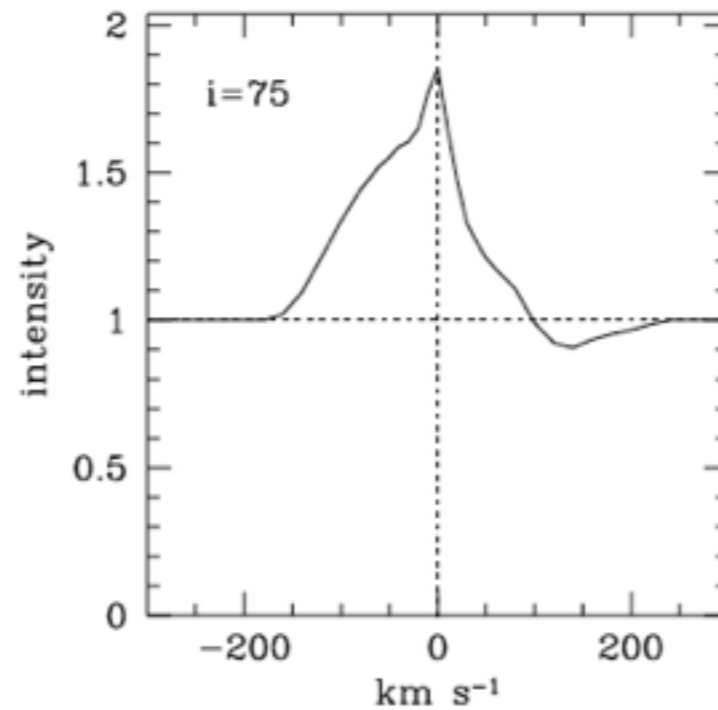
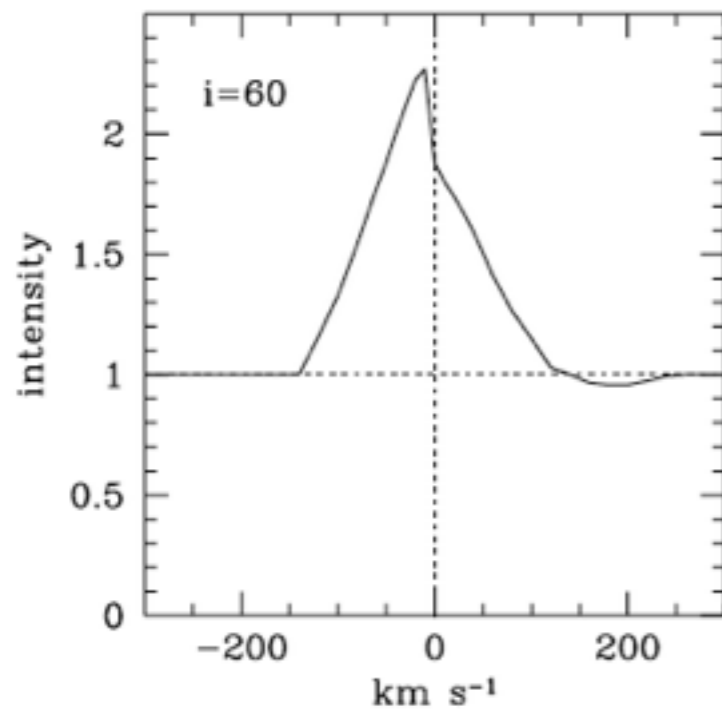
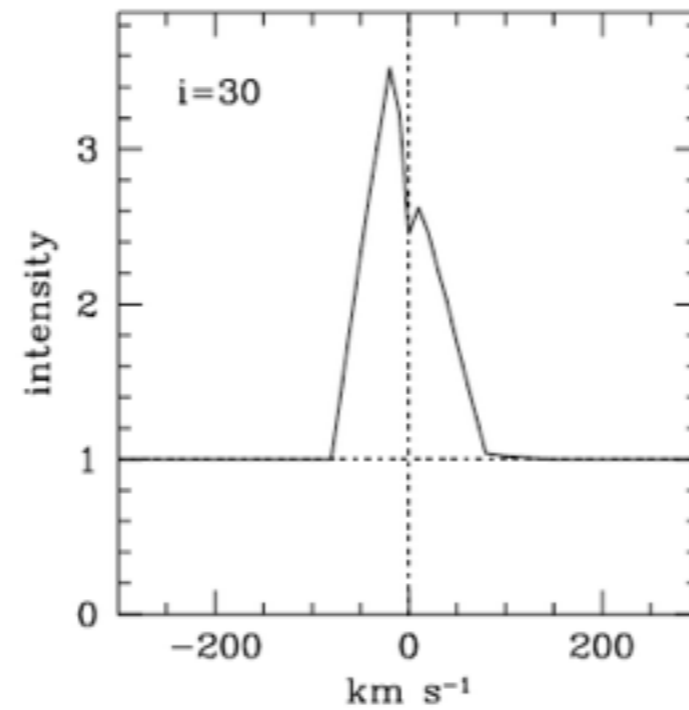
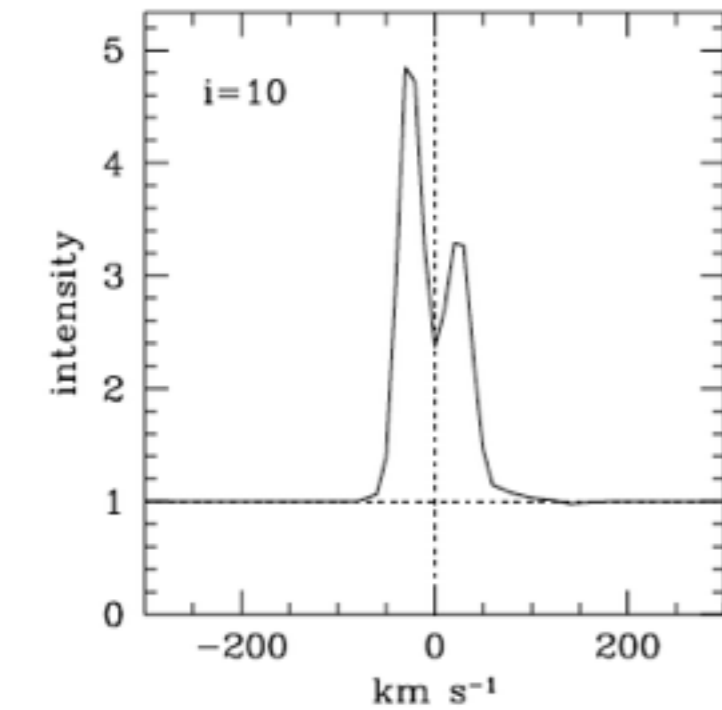


# Line shapes of Balmer lines

- ❖ The shapes of the Balmer lines are due to the velocity field and the geometry of the system
- ❖ line widths increase with inclination angle (los is aligned with the fastest part of the flow)
- ❖ Redshifted absorption is more pronounced at higher inclination (line of sight passes through increasing amount of infalling material)
- ❖ Emission at low velocities comes from both the regions of the flow nearest the disk and from material moving essentially perpendicular to the line of sight. This is by far the largest emitting volume and explains the centrally peaked nature of the profiles.



# Line shapes other than Balmer series



- ❖ The same shape as Balmer lines: common emitting region
- ❖ One might expect the Paschen and Brackett lines to form in a more limited volume of the magnetosphere closer to the star, but they are probably also optically thick...

# Parameter dependence of line fluxes

- ❖ Vary the accretion rate, gas temperature (characterized by the maximum value of the distribution), and the width and radial extent of the magnetosphere
- ❖ one parameter is changed while the others are held fixed (though not all are independent...)
- ❖ calculate total line flux (some lines in absorption)

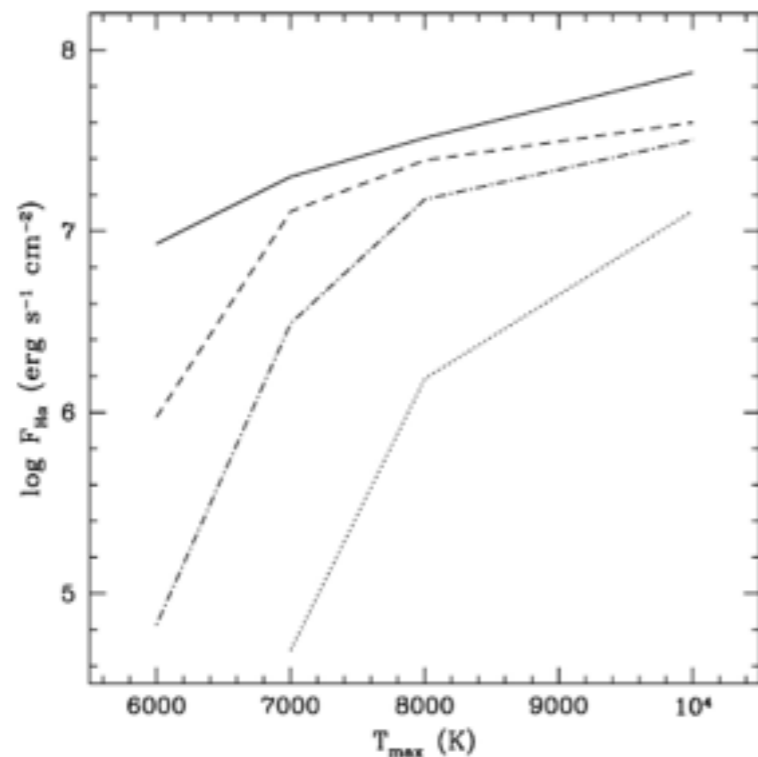


FIG. 6.—Model H $\alpha$  line fluxes for various temperature distributions (as defined by the maximum temperature) and accretion rates for a magnetosphere with  $r_{\text{mi}} = 2.2R_*$  and  $r_{\text{mo}} = 3R_*$ . The models are  $\dot{M} = 10^{-6} M_{\odot} \text{ yr}^{-1}$  (solid line),  $\dot{M} = 10^{-7} M_{\odot} \text{ yr}^{-1}$  (dashed line),  $\dot{M} = 10^{-8} M_{\odot} \text{ yr}^{-1}$  (dash-dotted line), and  $\dot{M} = 10^{-9} M_{\odot} \text{ yr}^{-1}$  (dotted line).

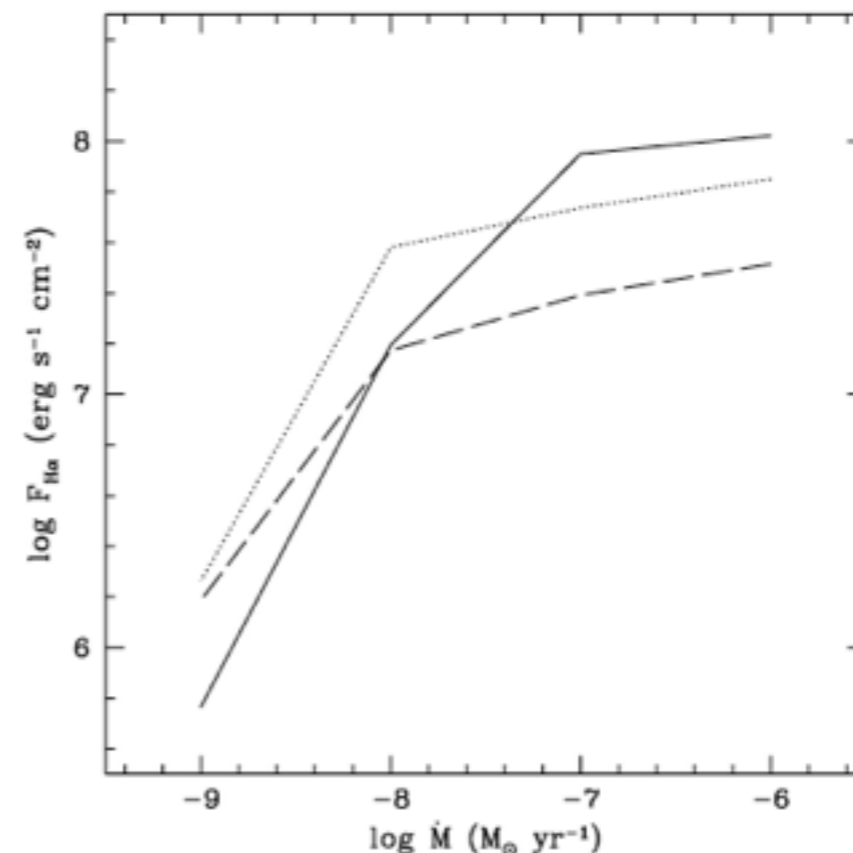


FIG. 7.—Model H $\alpha$  line fluxes as a function of accretion rate. The model values are  $r_{\text{mi}} = 4R_*$  and  $r_{\text{mo}} = 6R_*$  (solid line);  $r_{\text{mi}} = 5.2R_*$  and  $r_{\text{mo}} = 6R_*$  (dotted line); and  $r_{\text{mi}} = 2.2R_*$  and  $r_{\text{mo}} = 3R_*$  (dashed line). In each case,  $T_{\text{max}} = 8000 \text{ K}$ .

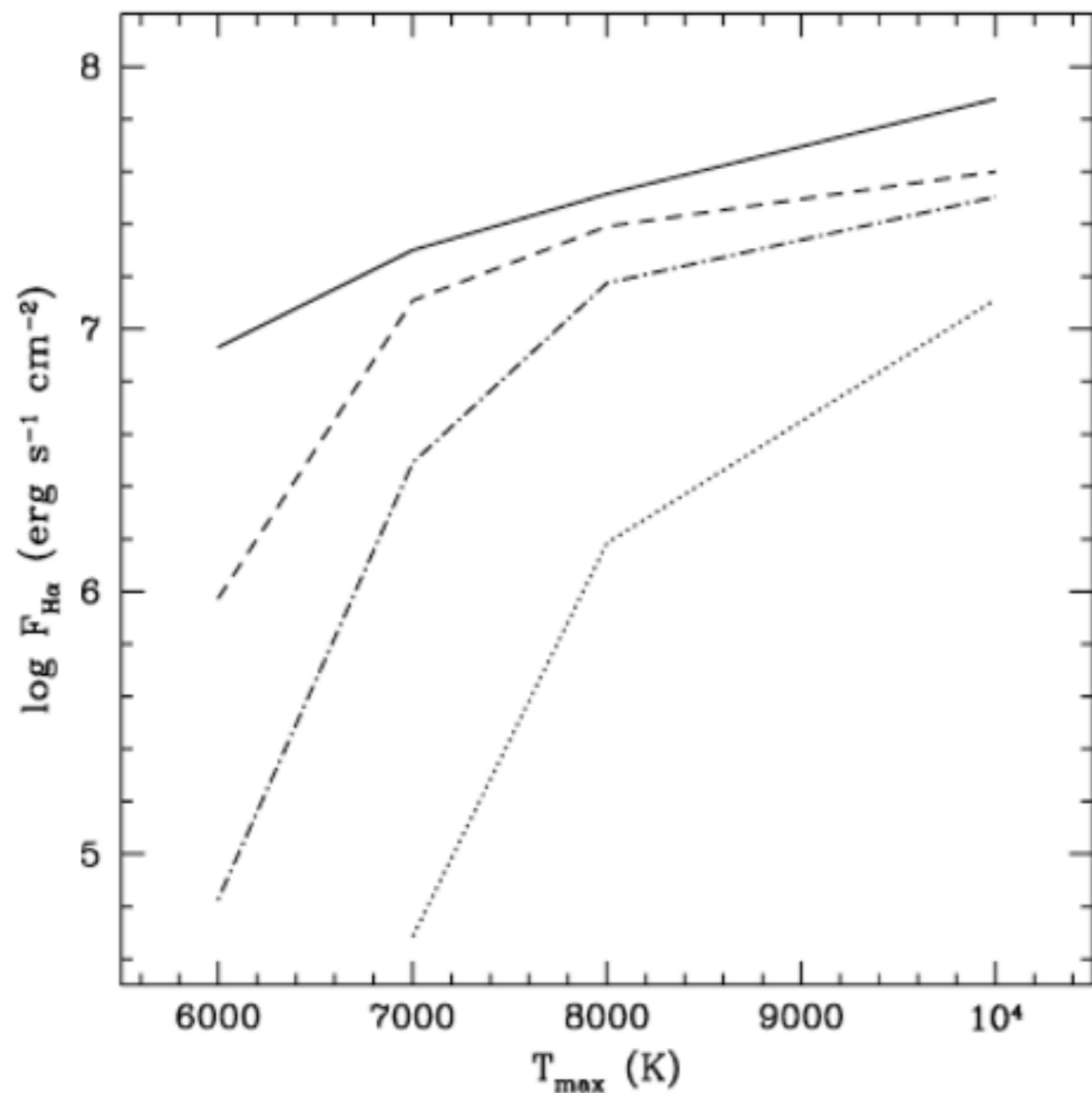


FIG. 6.—Model H $\alpha$  line fluxes for various temperature distributions (as defined by the maximum temperature) and accretion rates for a magnetosphere with  $r_{\text{mi}} = 2.2R_*$  and  $r_{\text{mo}} = 3R_*$ . The models are  $\dot{M} = 10^{-6} M_{\odot} \text{ yr}^{-1}$  (solid line),  $\dot{M} = 10^{-7} M_{\odot} \text{ yr}^{-1}$  (dashed line),  $\dot{M} = 10^{-8} M_{\odot} \text{ yr}^{-1}$  (dash-dotted line), and  $\dot{M} = 10^{-9} M_{\odot} \text{ yr}^{-1}$  (dotted line).

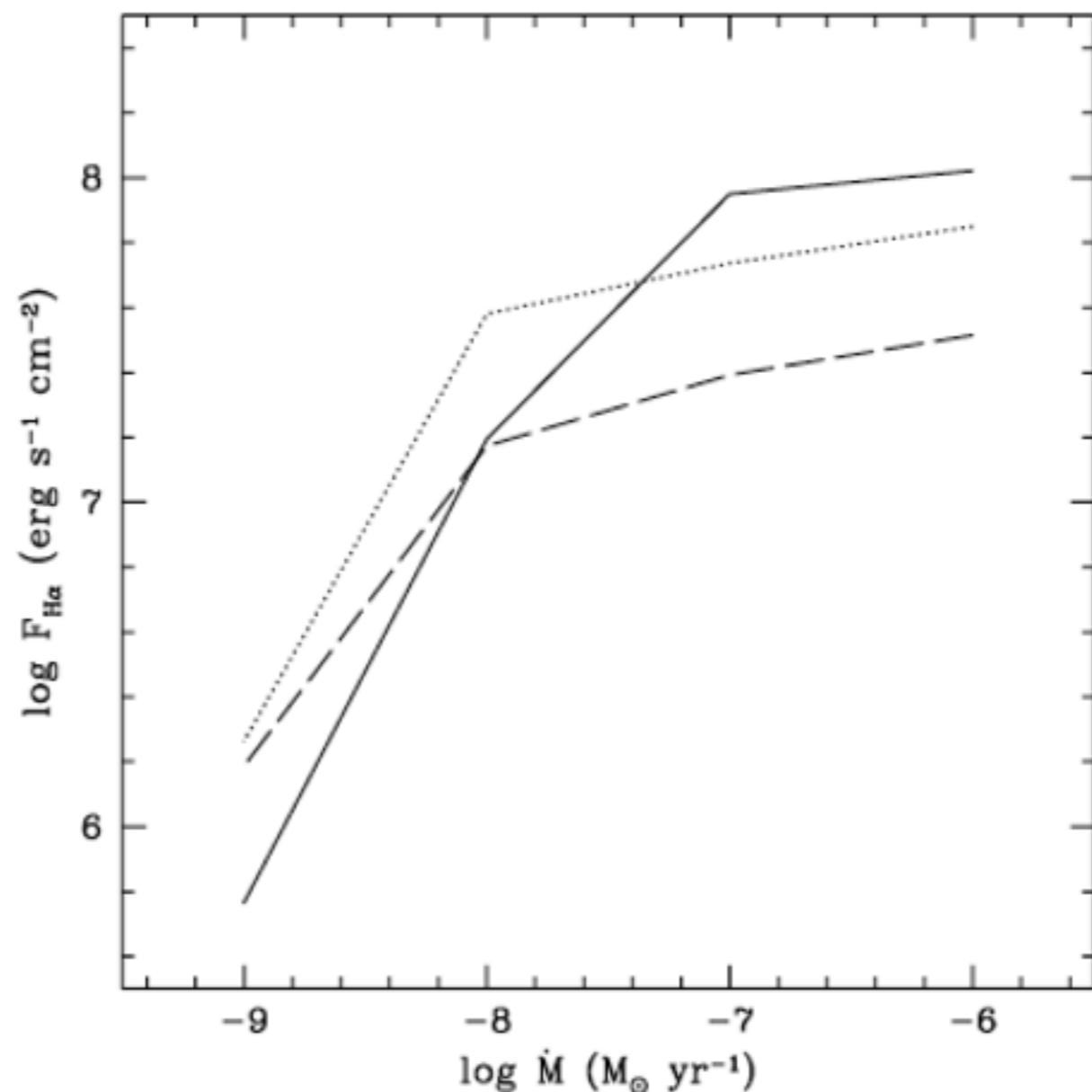


FIG. 7.—Model H $\alpha$  line fluxes as a function of accretion rate. The model values are  $r_{\text{mi}} = 4R_*$  and  $r_{\text{mo}} = 6R_*$  (solid line);  $r_{\text{mi}} = 5.2R_*$  and  $r_{\text{mo}} = 6R_*$  (dotted line); and  $r_{\text{mi}} = 2.2R_*$  and  $r_{\text{mo}} = 3R_*$  (dashed line). In each case,  $T_{\text{max}} = 8000 \text{ K}$ .

# Interpretation

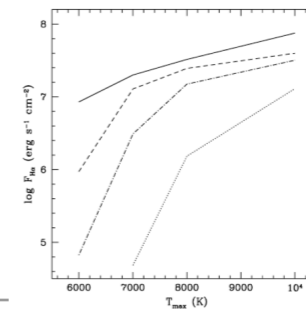


FIG. 6.—Model H $\alpha$  line fluxes for various temperature distributions (as defined by the maximum temperature) and accretion rates for a magnetosphere with  $r_{\text{in}} = 2.2R_*$  and  $r_{\text{out}} = 3R_*$ . The models are  $\dot{M} = 10^{-7} M_{\odot} \text{ yr}^{-1}$  (solid line),  $\dot{M} = 10^{-7} M_{\odot} \text{ yr}^{-1}$  (dashed line),  $\dot{M} = 10^{-8} M_{\odot} \text{ yr}^{-1}$  (dash-dotted line), and  $\dot{M} = 10^{-9} M_{\odot} \text{ yr}^{-1}$  (dotted line).

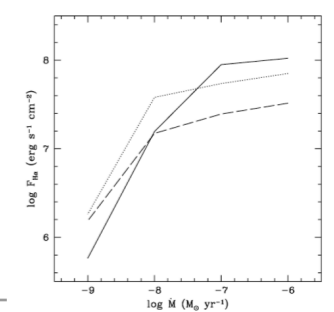
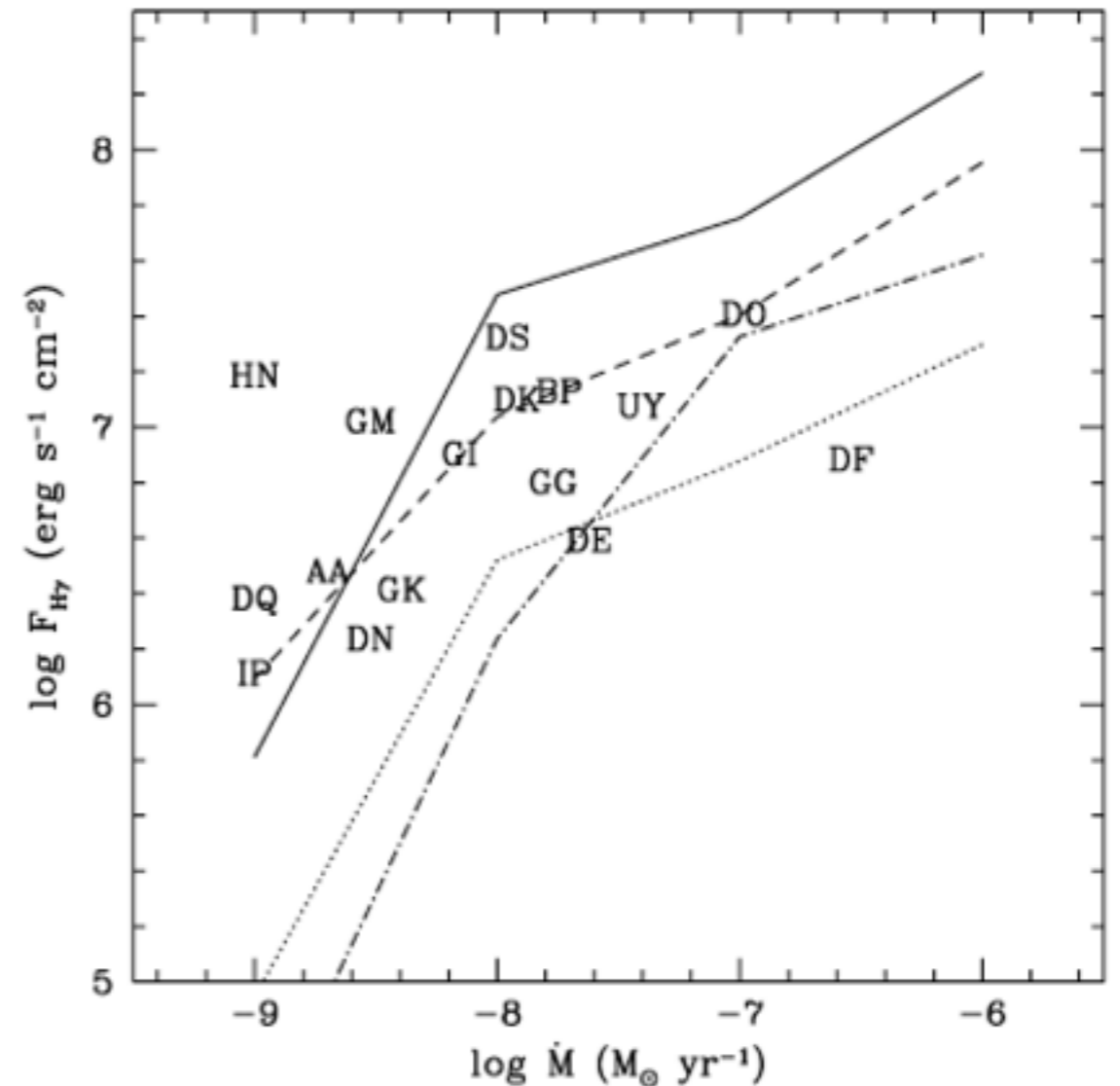
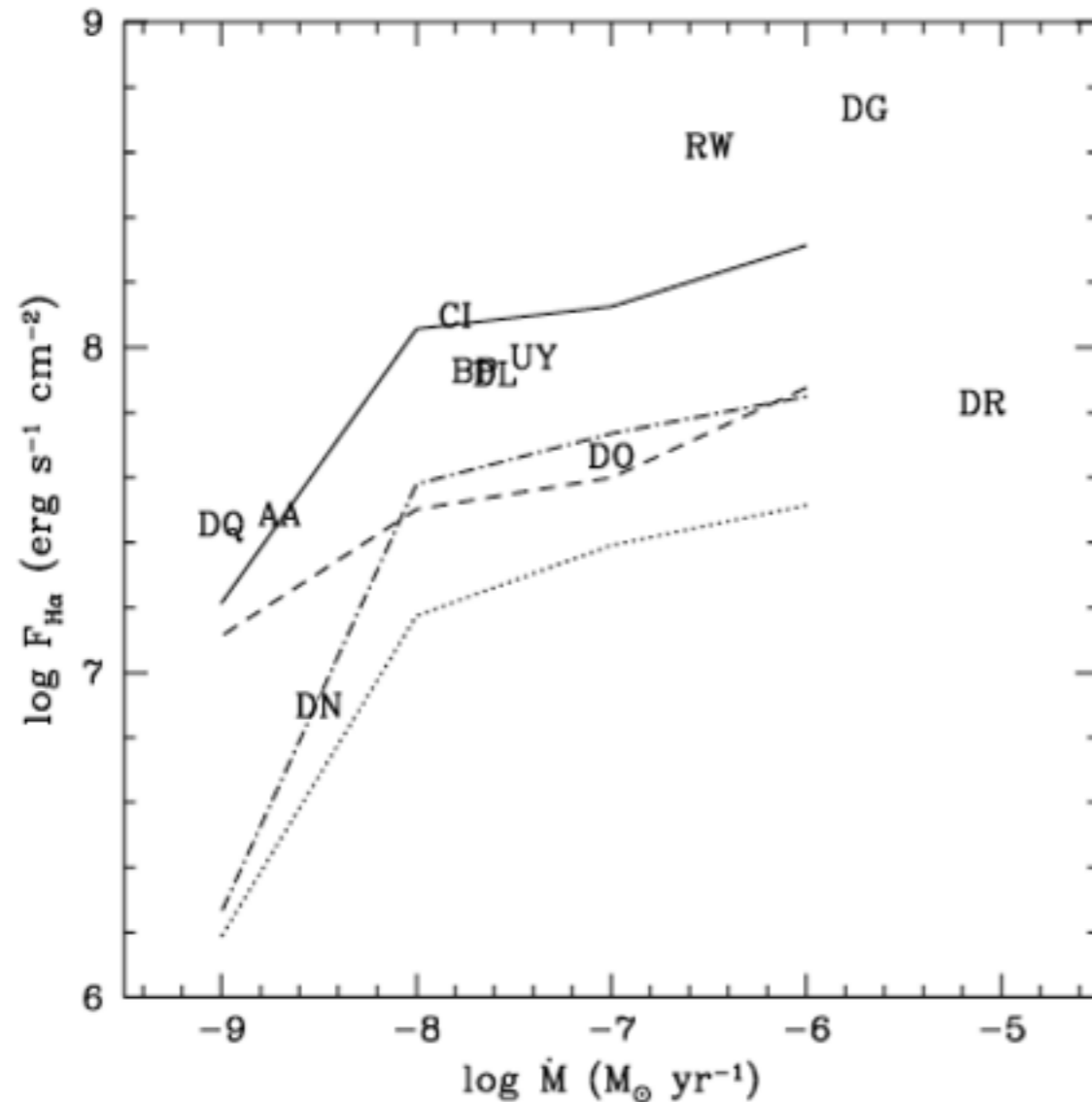


FIG. 7.—Model H $\alpha$  line fluxes as a function of accretion rate. The model values are  $r_{\text{in}} = 4R_*$  and  $r_{\text{out}} = 6R_*$  (solid line);  $r_{\text{in}} = 5.2R_*$  and  $r_{\text{out}} = 6R_*$  (dotted line); and  $r_{\text{in}} = 2.2R_*$  and  $r_{\text{out}} = 3R_*$  (dashed line). In each case,  $T_{\text{max}} = 8000 \text{ K}$ .

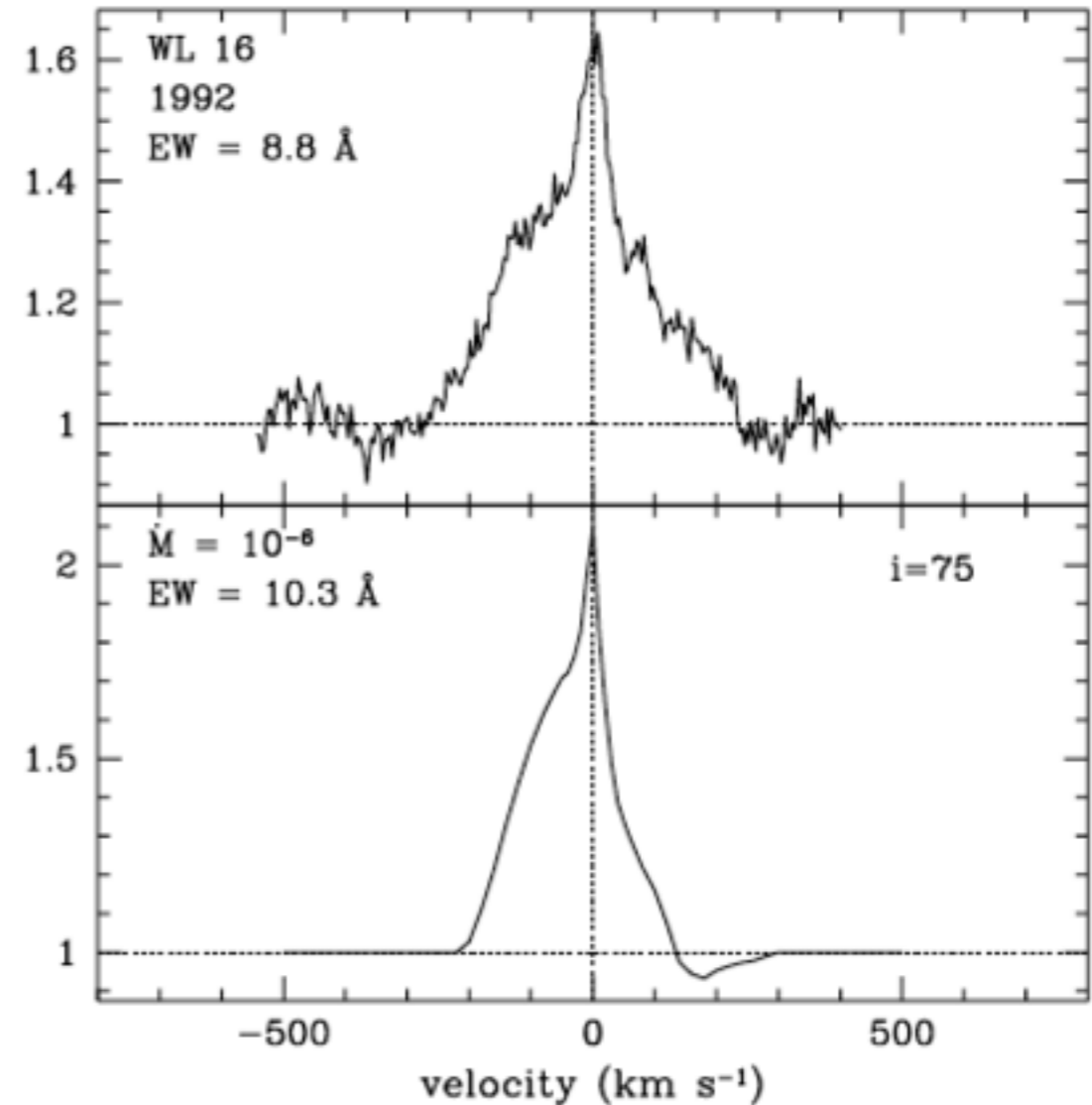
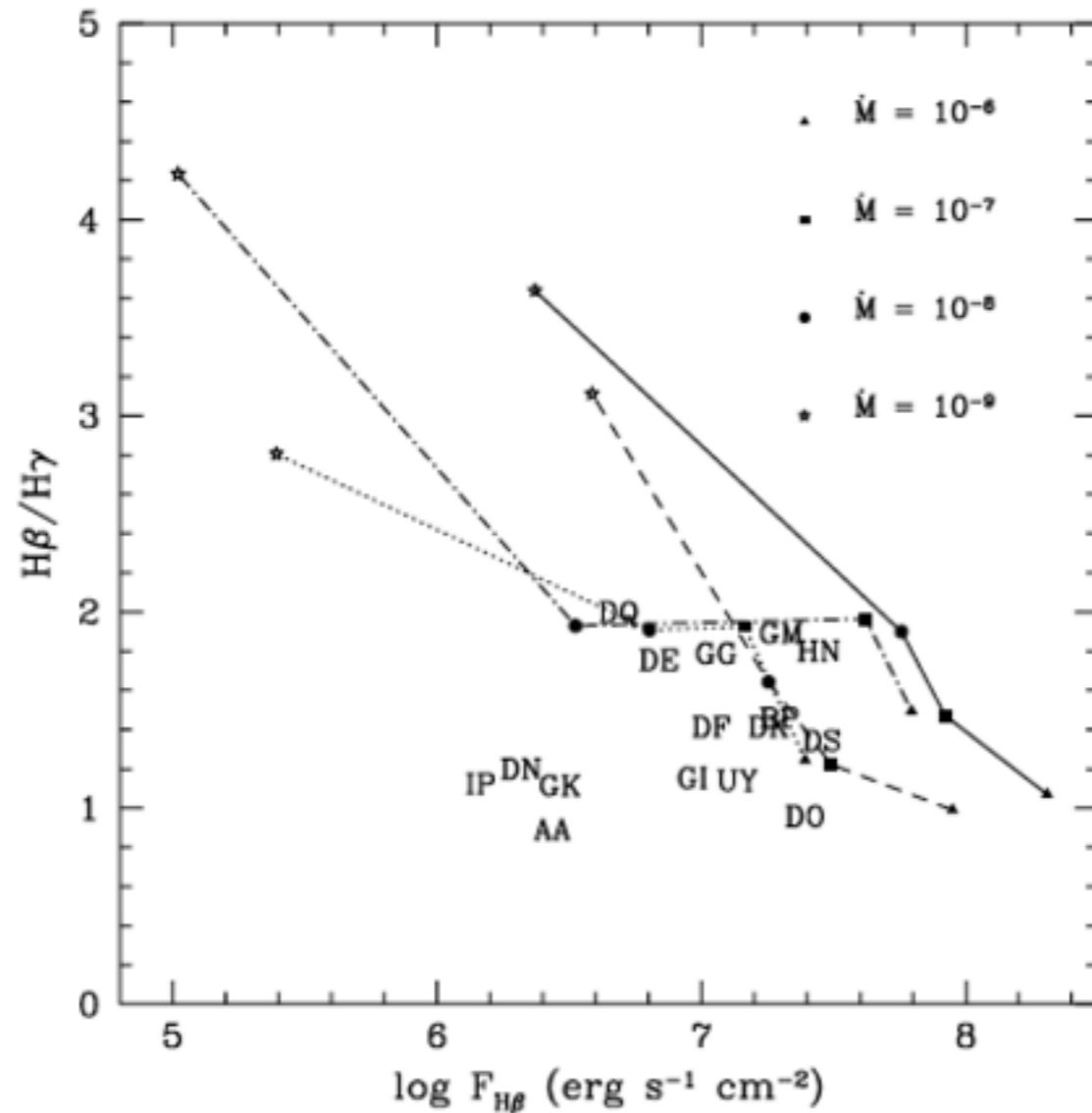
- ❖ Vary the accretion rate, gas temperature (characterized by the maximum value of the distribution), and the width and radial extent of the magnetosphere
- ❖ one parameter is changed while the others are held fixed (though not all are independent...). Calculate total line flux.
- ❖ At low accretion rates, the flux decreases dramatically with decreasing accretion rate because there is a fairly sharp drop in the line optical depth, and the emission essentially goes away (this behavior is striking in the line profiles, which become either flat topped or completely in absorption).
- ❖ The slope in the line flux as a function of accretion rate becomes shallower at higher accretion rates because of the increasing thermalization of the lines.
- ❖ At high enough densities, the magnetosphere would become a completely optically thick blackbody, with the emergent flux coming only from the outer surface. The H $\alpha$  line fluxes would only be good accretion rate indicators for objects with the lowest accretion rates.

# Comparison with observations



- ❖ Goal: determine if the magnetospheric model can explain the observed range of line fluxes and accretion rate estimates and proceed to constrain the uncertain magnetospheric physical parameters (size, width, temperature)

# Comparison with observations



❖ low accretion objects: shock effect?

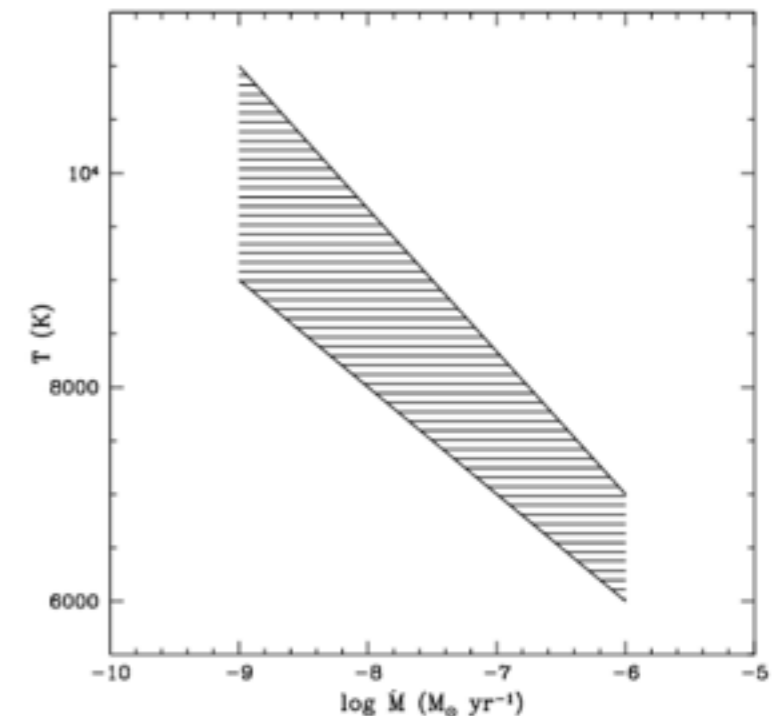
❖ Possible problem for the highest accretion objects: strong winds

❖ Broad profiles: Stark broadening?

❖ Halfa: high optical depth

# Constraining the temperature

- ❖ What is the temperature structure of the magnetosphere?
- ❖ No theory of heating the infalling gas...
- ❖ Heating sources: Balmer photoionization, adiabatic compression due to the converging field lines
- ❖ Cooling is dominated by Ca II and Mg II line emission
- ❖ Only these processes would yield too low temperatures
- ❖ Additional heating sources: magnetically driven effects
- ❖ Models with too low temperature produce too low line fluxes
- ❖ Upper limit for the temperature comes from gas continuum. Too high temperatures would produce too high continuum and no lines. But we see lines.

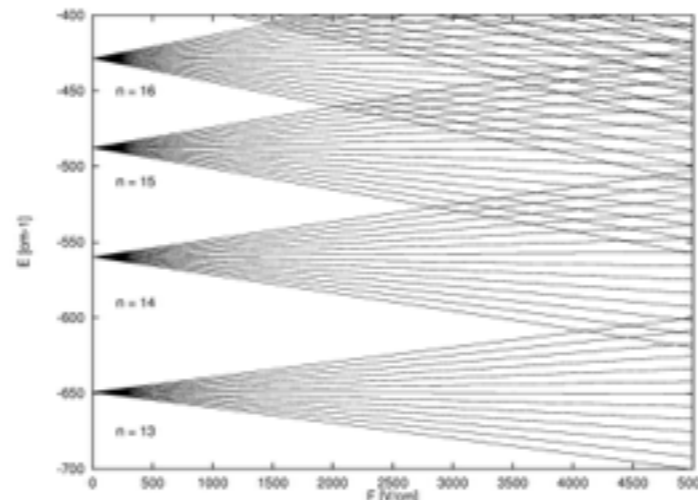




# Effects of Stark Broadening

---

- ❖ One of the major discrepancies between the model results and the observations is the H $\alpha$  emission.
- ❖ The model is not able to reproduce the substantial line wings (typically  $\sim 500$  km s $^{-1}$ ) seen in the H $\alpha$  profiles of many CTTSs.
- ❖ Likely source of the broad wings is Stark broadening
- ❖ Slab model calculations:
  - ❖ the contribution from Stark broadening from the infalling gas is small for all but the largest accretion rates ( $10^{-6}$  M yr $^{-1}$ ).



# Accretion rate diagnostic

---

- ❖ The ultimate goal in studying the emission lines is to obtain some diagnostic of the accretion rate.
- ❖ Complications:
  - temperature and size (including both the outer radius and width) of the magnetosphere are important factors
  - the Balmer lines and Br $\gamma$  are all optically thick at higher accretion rates, no dependence on gas density
- ❖ More optically thin lines would be great
- ❖ The last Paschen and Brackett lines visible in emission in a CTTS spectrum may correlate with the accretion rate
- ❖ Emission lines of other atomic species, observed profiles of some O I and Na I lines, as well as the broad components of He I and Ca II

# EMISSION-LINE DIAGNOSTICS OF T TAURI MAGNETOSPHERIC ACCRETION. I. LINE PROFILE OBSERVATIONS

JAMES MUZEROLLE, LEE HARTMANN, NURIA CALVET  
Astronomical Journal, Volume 116, 455 (1998)

---

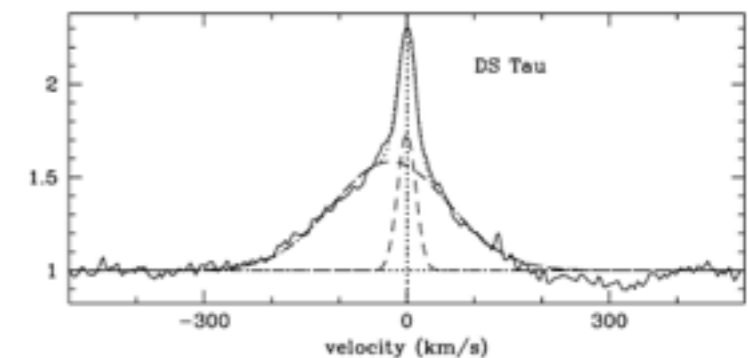
Ábrahám Péter

Accretion processes, 2014. november 5.

# Magnetospheric accretion

---

- ❖ the best explanation for the rich emission-line T Tauri spectrum (atomic hydrogen and metallic permitted and forbidden lines)
- ❖ NOT enhanced chromospheric activity; outflowing winds, nor turbulence in a boundary layer
- ❖ hydrogen emission lines originate in the infall zone (line profiles with large (several hundred  $\text{km s}^{-1}$ ) line widths, blue asymmetries, redshifted absorption components, depending on the geometry of the system)
- ❖ the formation of most of the metallic emission lines is also related in some way to the accretion process.
  - broad line profile, typically with widths in excess of  $100 \text{ km s}^{-1}$ , which is often asymmetric, with blue shifted and/or redshifted absorption components. Possible origin: accretion flow
  - narrow profile centered at line center, often superposed on top of a broad component. Possible origin: hot chromosphere.



# Observations

---

- ❖ 11 classical T Tauri stars (plus 1 WTTS, LkCa 7)
- ❖ represent a wide range of accretion rates (and veiling)
- ❖ echelle spectrograph on the 4 m telescope at KPNO
- ❖ spectral coverage 5800 to 9000 Å
- ❖  $R \sim 35,000$

Object	Spectral Type	$A_V$	$\log \dot{M}(M_\odot \text{ yr}^{-1})$
AA Tau .....	K7	0.74	-8.48
BP Tau .....	K7	0.51	-7.54
CW Tau .....	K3	2.4 <sup>a</sup>	-8.8 <sup>a</sup>
DG Tau .....	K7-M0	1.0 <sup>a</sup>	-5.7 <sup>b</sup>
DL Tau .....	K7	1.35 <sup>a</sup>	-7.63 <sup>a</sup>
DN Tau .....	M0	0.25	-8.46
DR Tau .....	K7	1.0 <sup>a</sup>	-5.1 <sup>b</sup>
DS Tau .....	K5	0.34	-7.89
GK Tau .....	K7	0.94	-8.19
RW Aur .....	K3	1.2 <sup>a</sup>	-6.47 <sup>a</sup>
UY Aur .....	K7	1.26	-7.18

# Observations

---

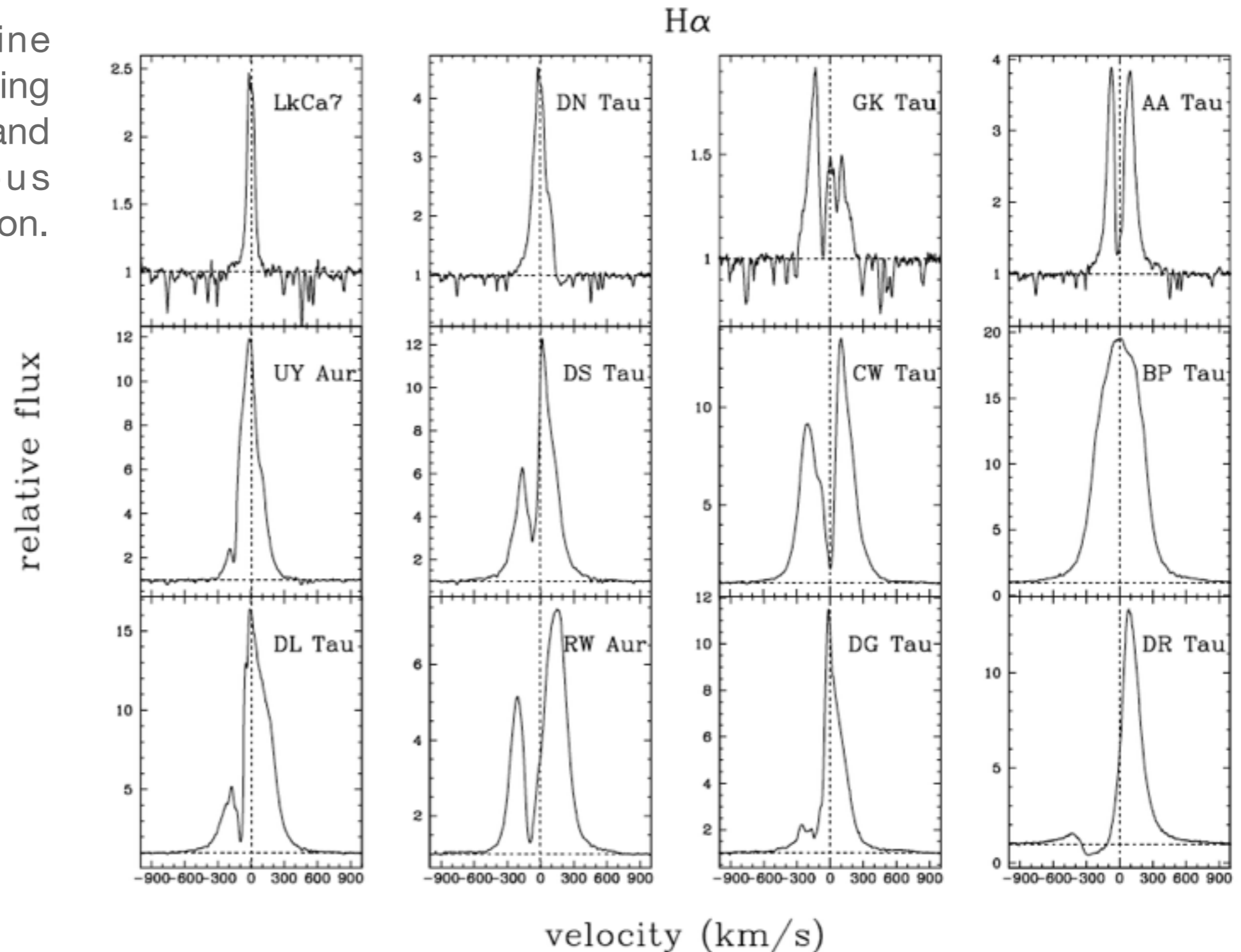
- ❖ Subtract photosphere
- ❖ one must first subtract out the underlying photospheric absorption spectrum
- ❖ Use the WTTS template to estimate veiling
- ❖ The depths of absorption lines in a 15 Å interval of the template spectrum are compared with those of the object using a chi<sup>2</sup> minimization routine
- ❖ Determine an additive constant: the veiling

$$r = F_{\text{veil}}/F_{\text{phot}}$$

- ❖ The procedure removes photosphere AND computes veiling

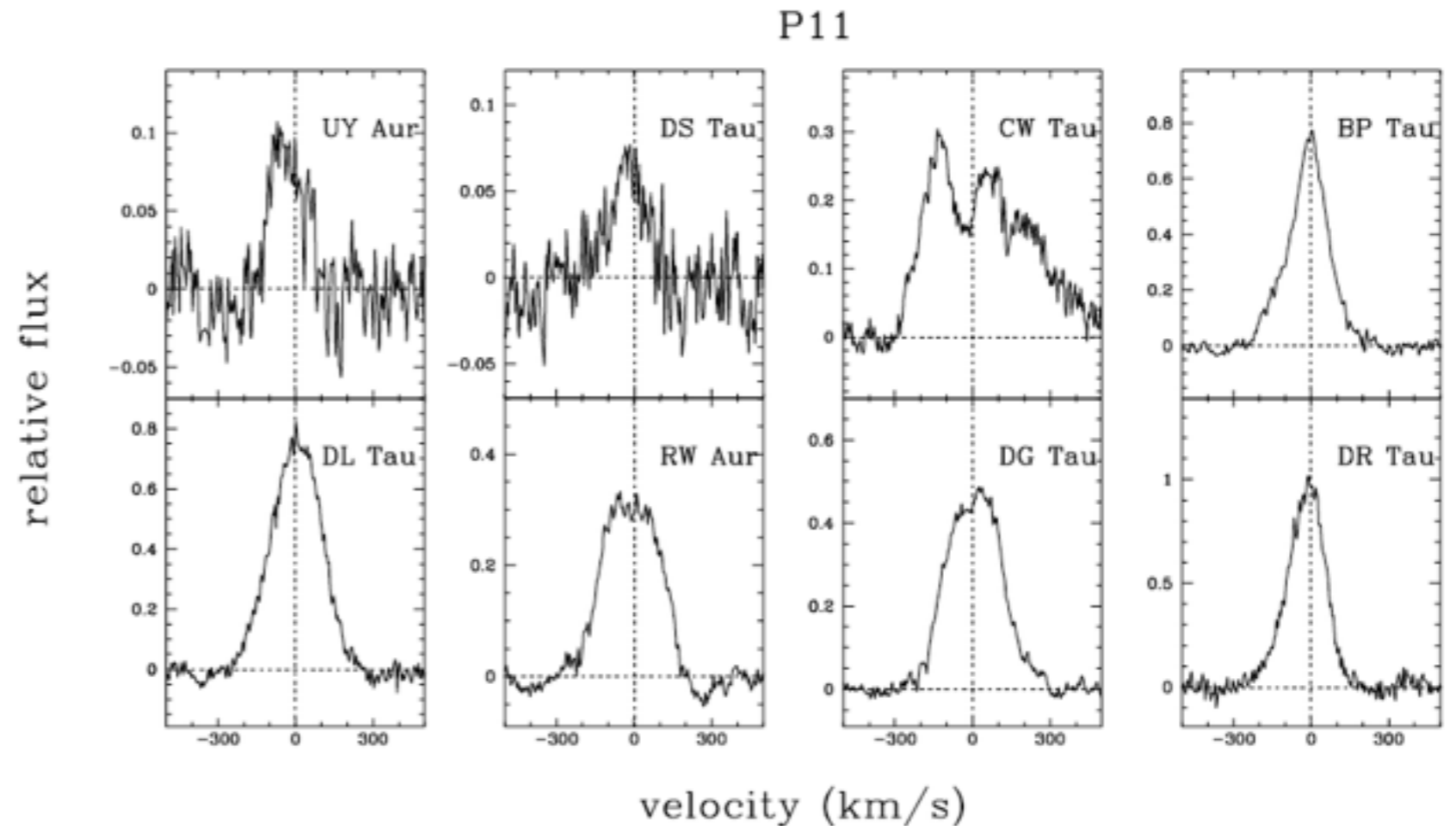
# Spectral profiles: hydrogen

- ❖ H $\alpha$ : very large line wings often extending beyond 500 km/s and almost ubiquitous blueshifted absorption.



# Spectral profiles: hydrogen

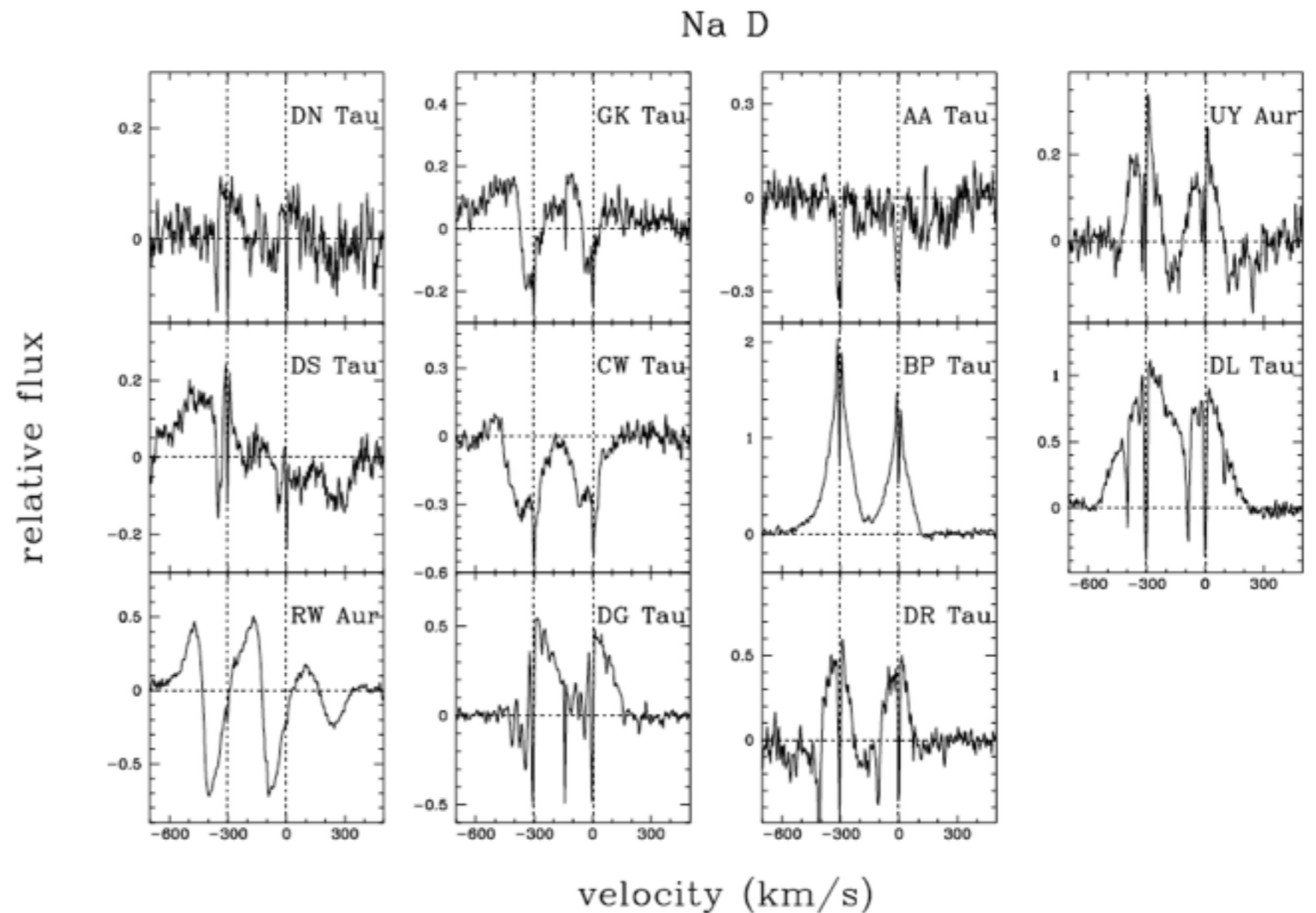
- ❖ Many Paschen lines are contaminated
- ❖ Pa11: some similarities to Balmer lines: large line widths (FWHM~200 km/s), central peaks, blueward asymmetry
- ❖ But NO blueshifted absorption (similarly to Pa beta and Br gamma)
- ❖ symmetric peak, inconsistent with magnetospheric models
- ❖ For stars with highest veiling, Pa series is in emission up to P24





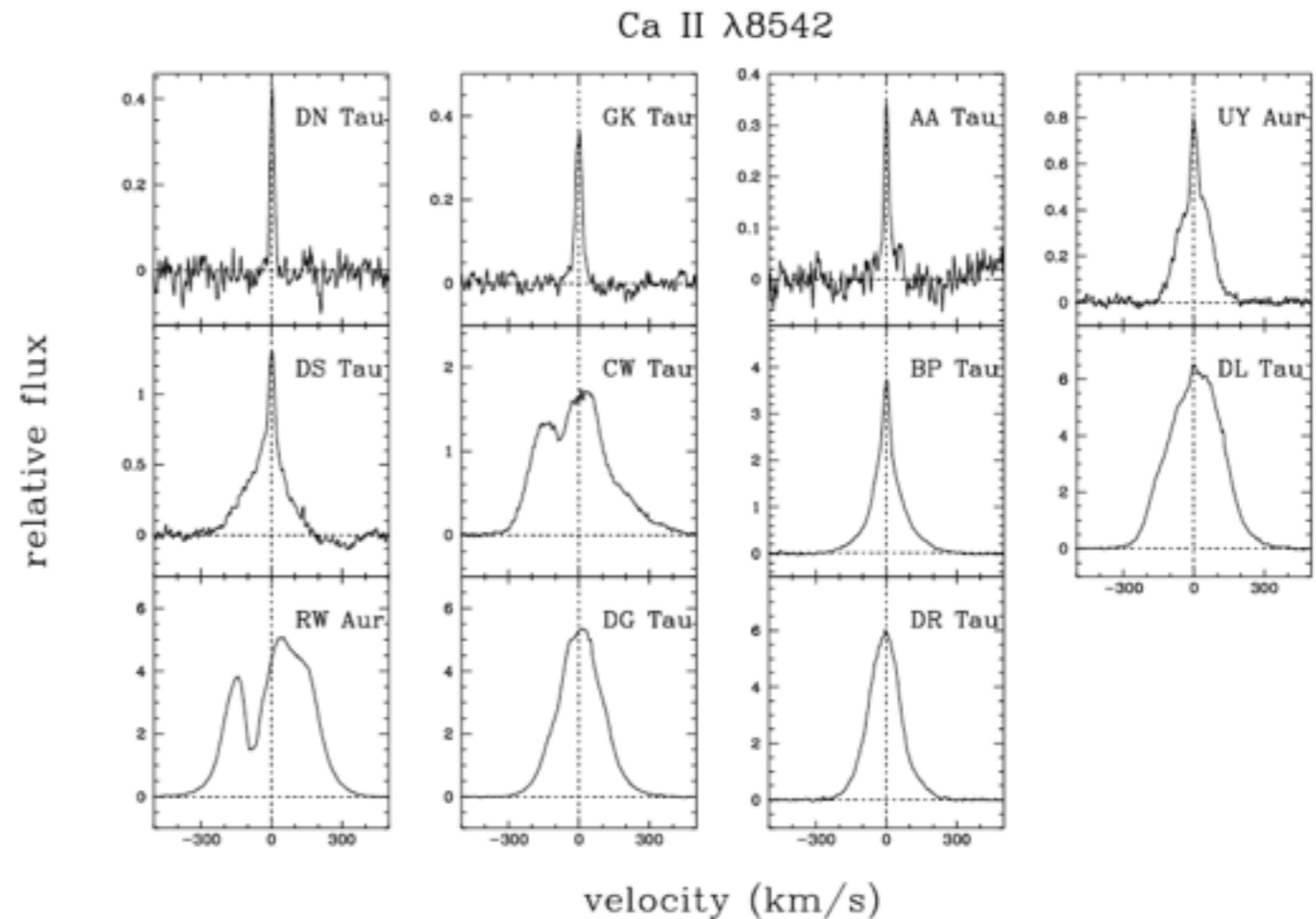
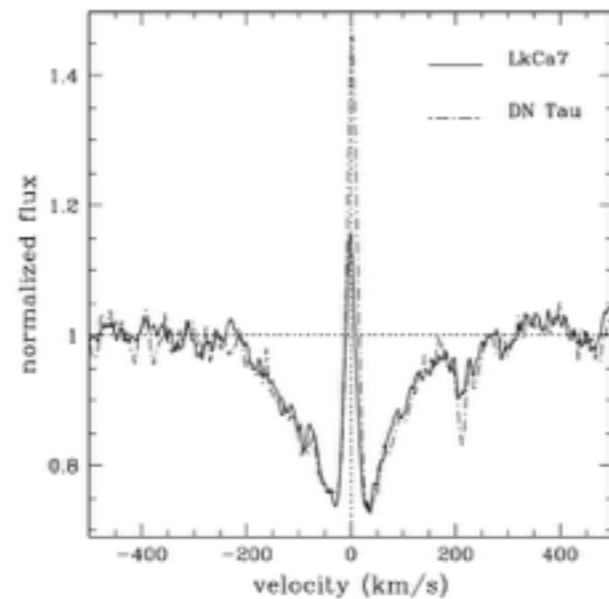
# Spectral profiles: sodium (Na D)

- ❖ Broad emission, evidence for infall (BP Tau, UY Aur, and DR Tau)
- ❖ 5 cases with redshifted absorption (infall signature)
- ❖ In many cases lines are contaminated by blueshifted absorption (not optimal infall indicators). Only BP Tau lacks any contamination



# Spectral profiles: Ca II

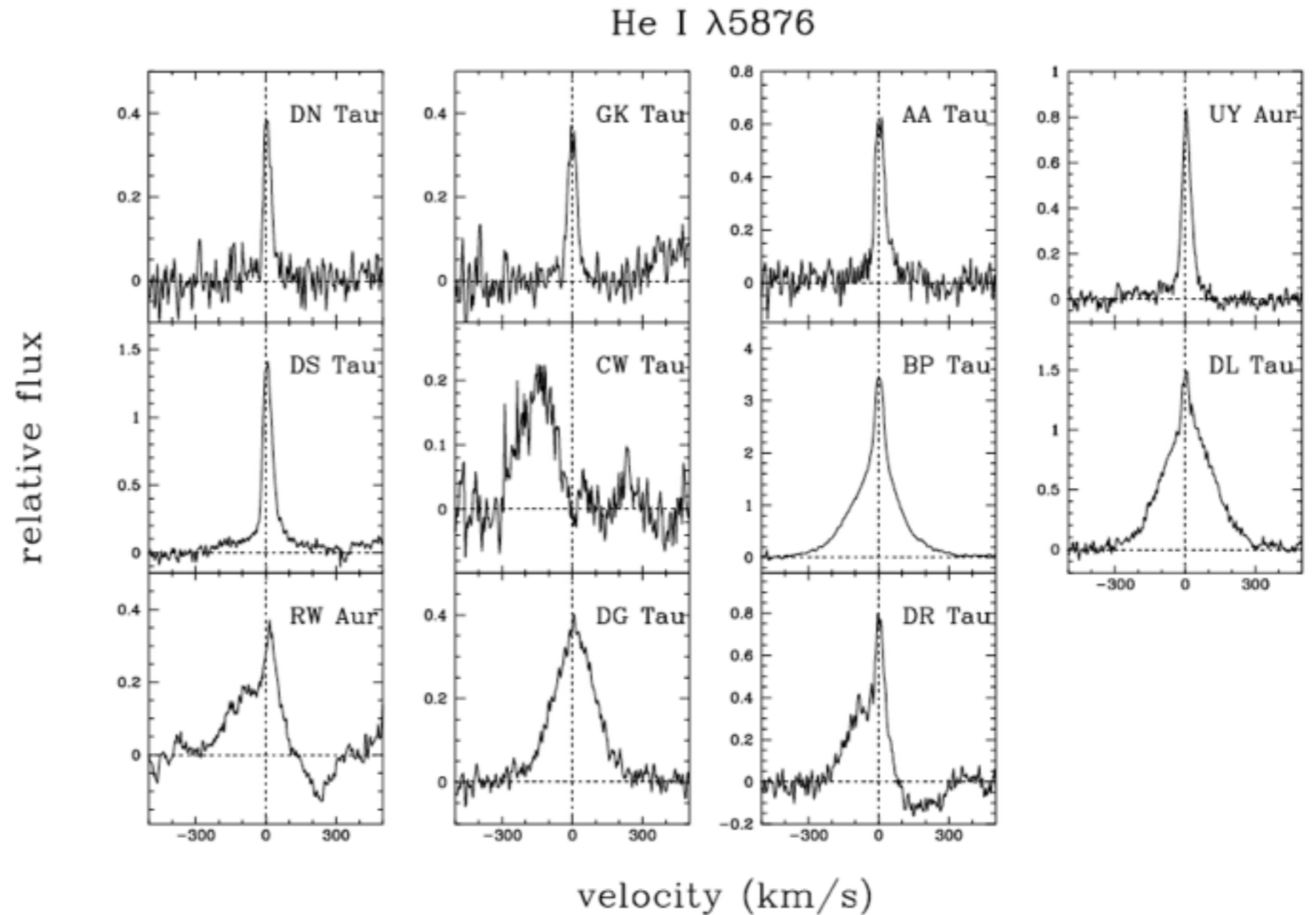
- ❖ Ca II infrared triplet
- ❖ Strong emission
- ❖ Low veiling (unsubtracted spectra)



- ❖ chromospheric model
- ❖ B and N components, B, N, and BN morphologies
- ❖ B dominates at high veiling
- ❖ Blending with Pa lines

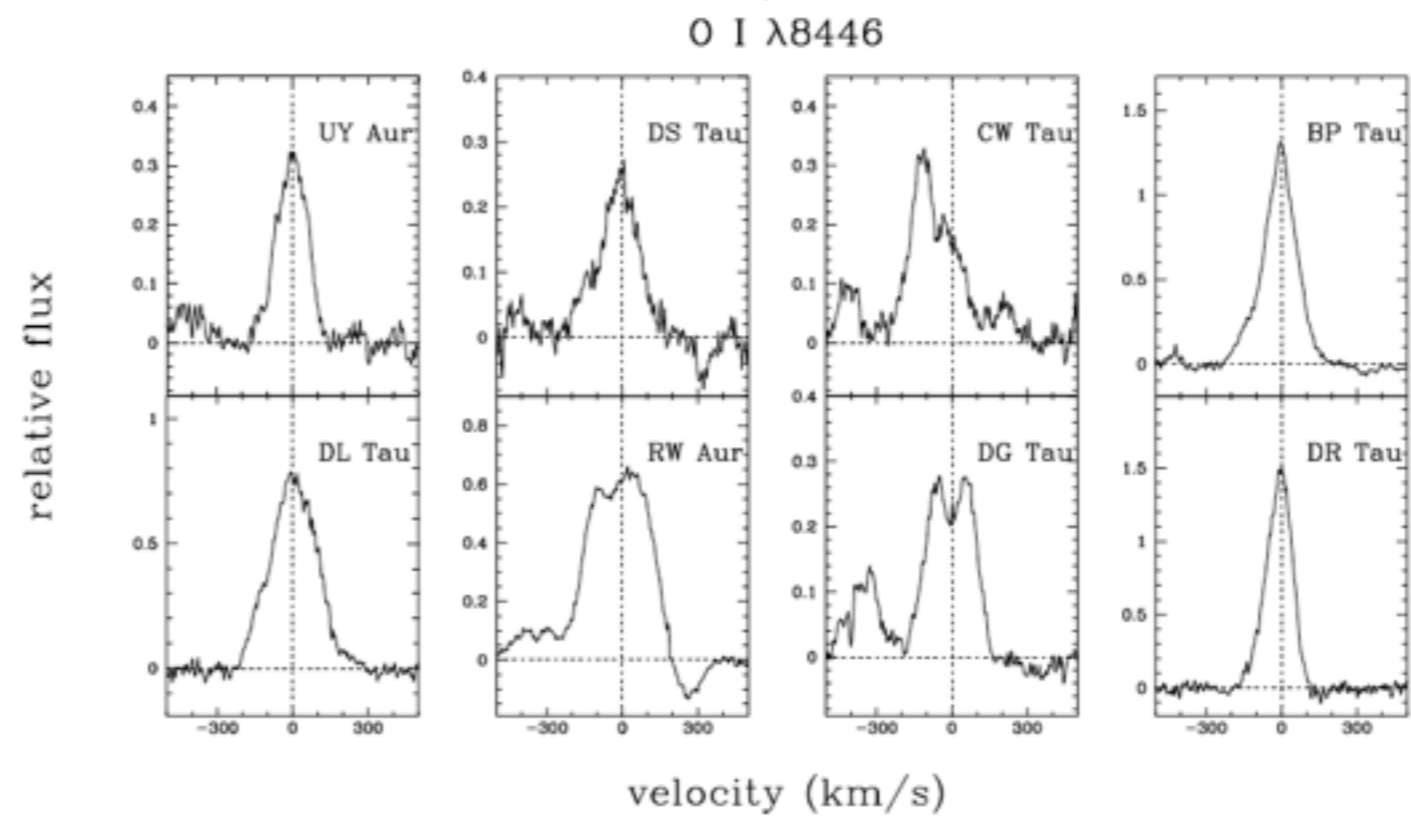
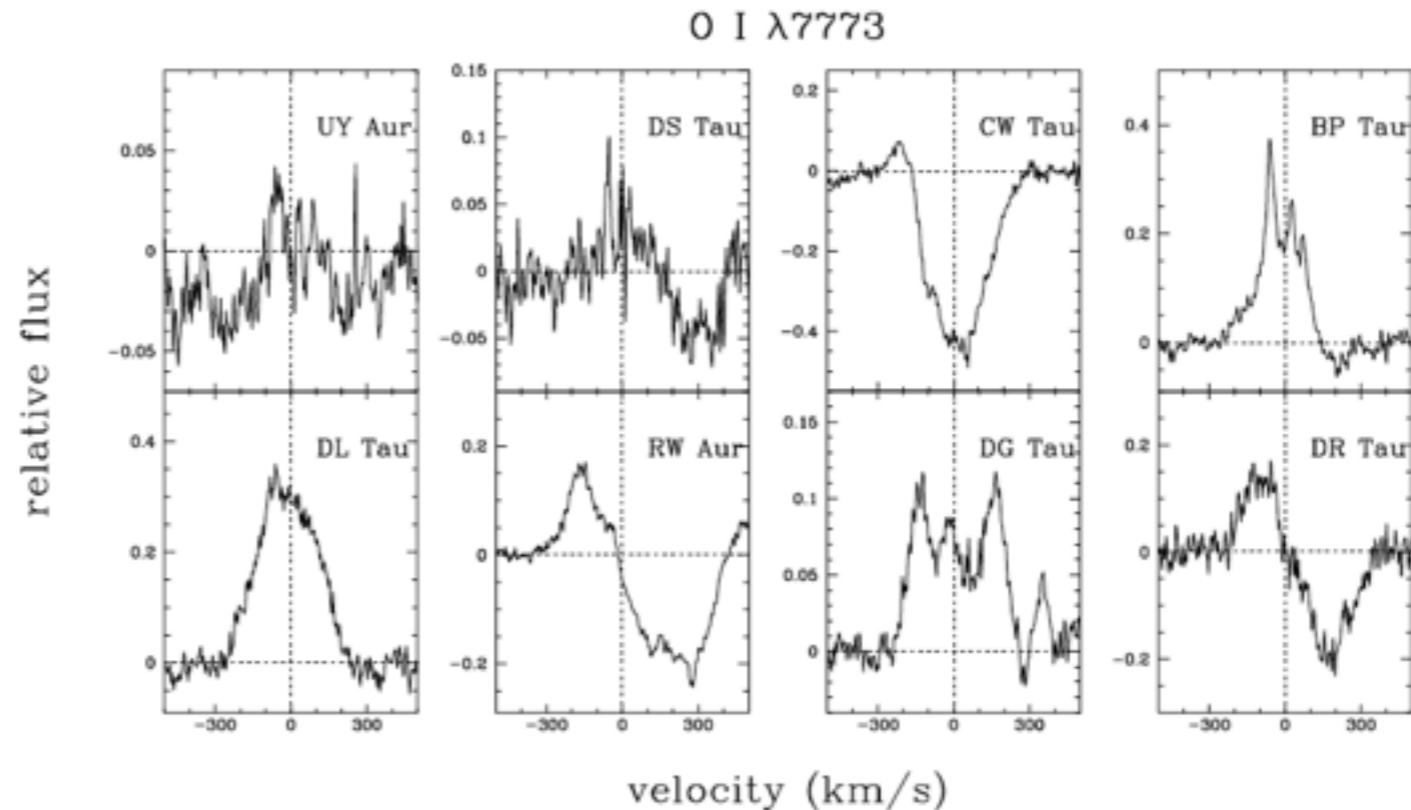
# Spectral profiles: He I

- ❖ Qualitatively like the Ca II triplet
- ❖ N and B components
- ❖ N does not disappear at high veiling (unlike Ca)



# Spectral profiles: O I 7773 AA and 8446 AA

- ❖ Permitted atomic oxygen lines
- ❖ the 7773 AA line is more sensitive for infall
- ❖ BP Tau: triplet resolved



# Profile decomposition (Ca II, He I)

- ❖ Try to separate N and B components
- ❖ Contamination from Pa lines
- ❖ For the broad component: no Gaussian fit, but subtraction of all other components
- ❖ Determine FWHM and peak flux
- ❖ In many cases the subtracted broad component shows infall characteristics

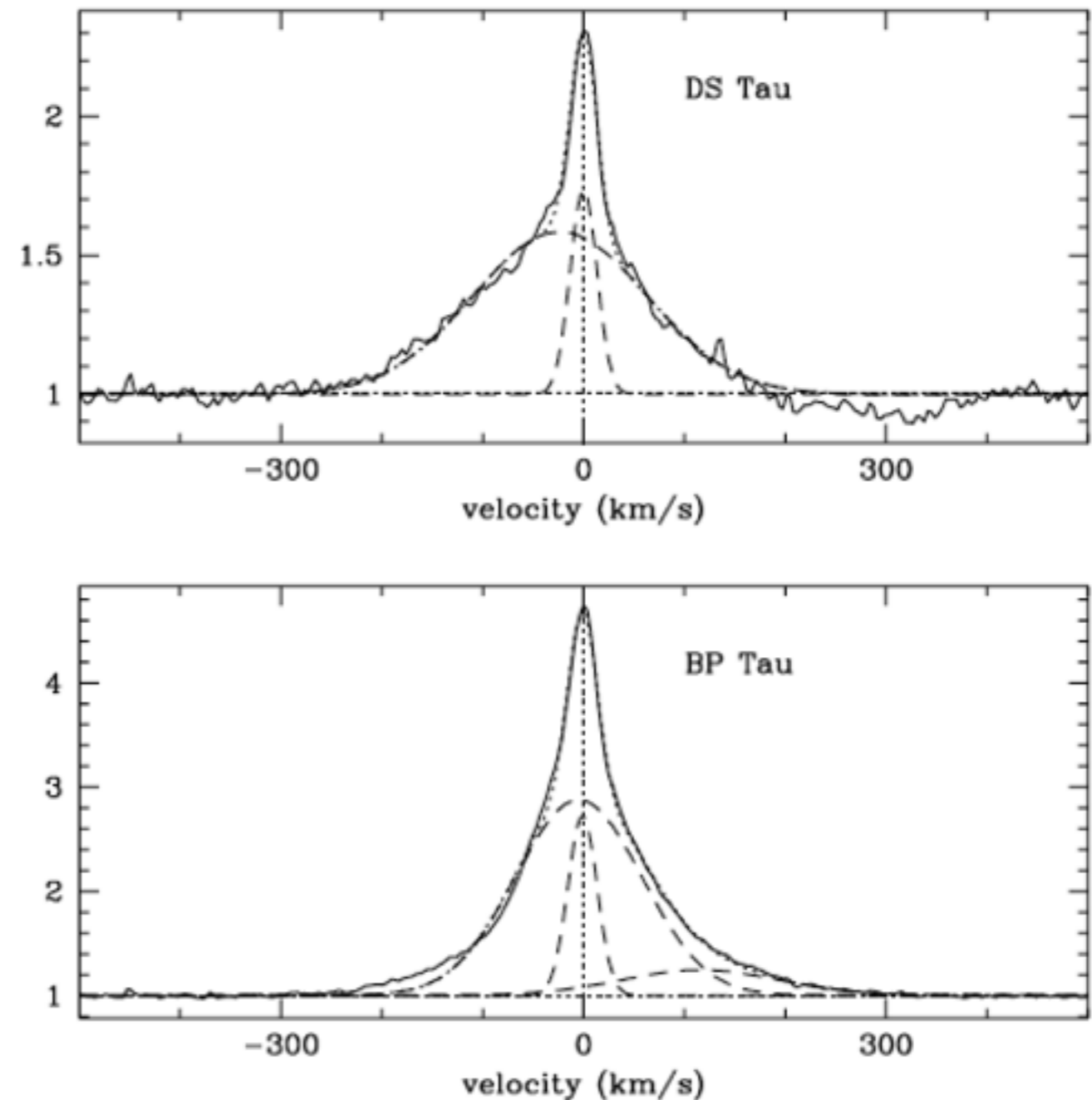
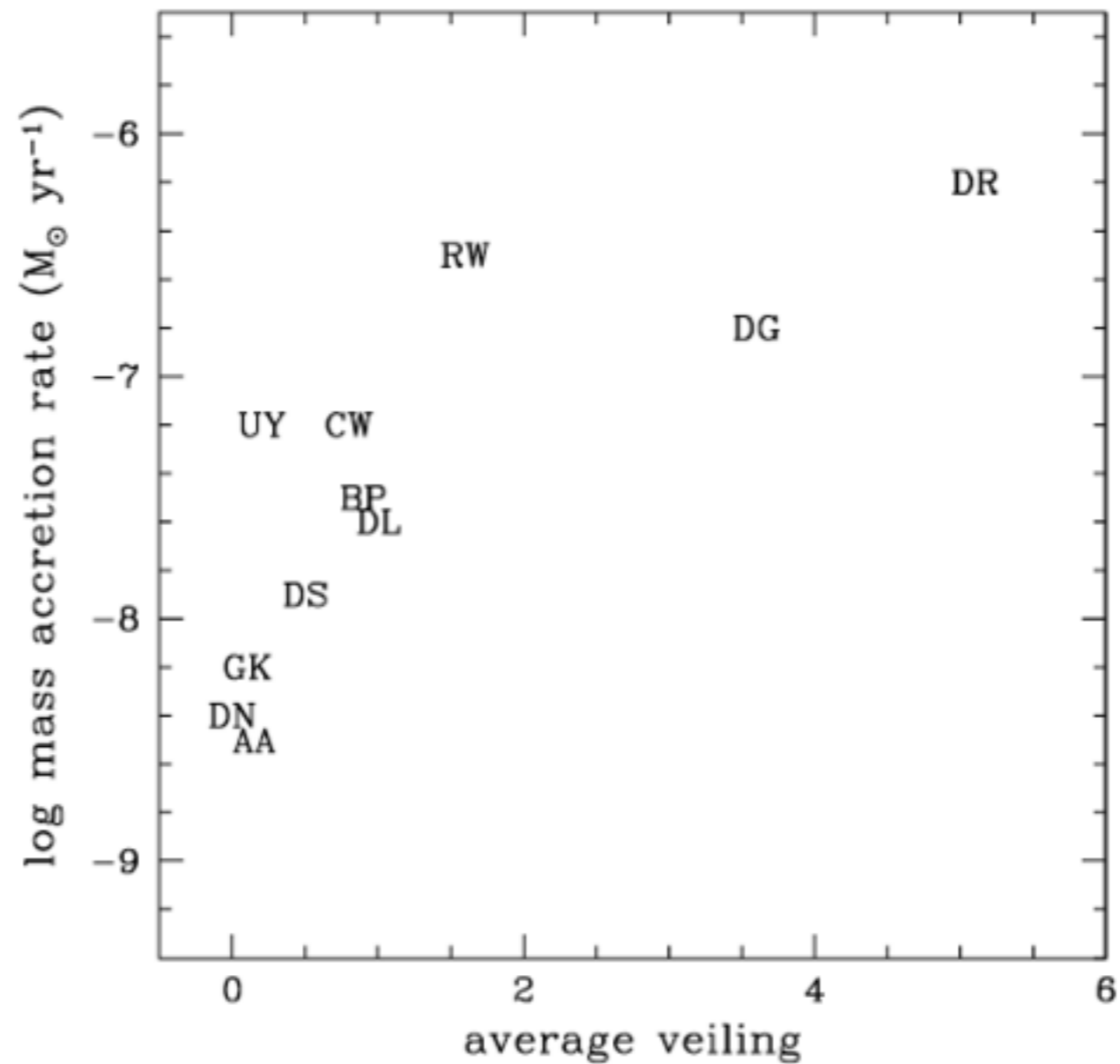


FIG. 3.—Decomposition of the Ca II  $\lambda 8542$  line profile. Dashed lines show the Gaussian fits—note the third component in BP Tau, representing the blended Pa15 line.

# Correlations

- ❖ Average veiling vs. accretion rate from the literature (blue excess, e.g. GHBC)

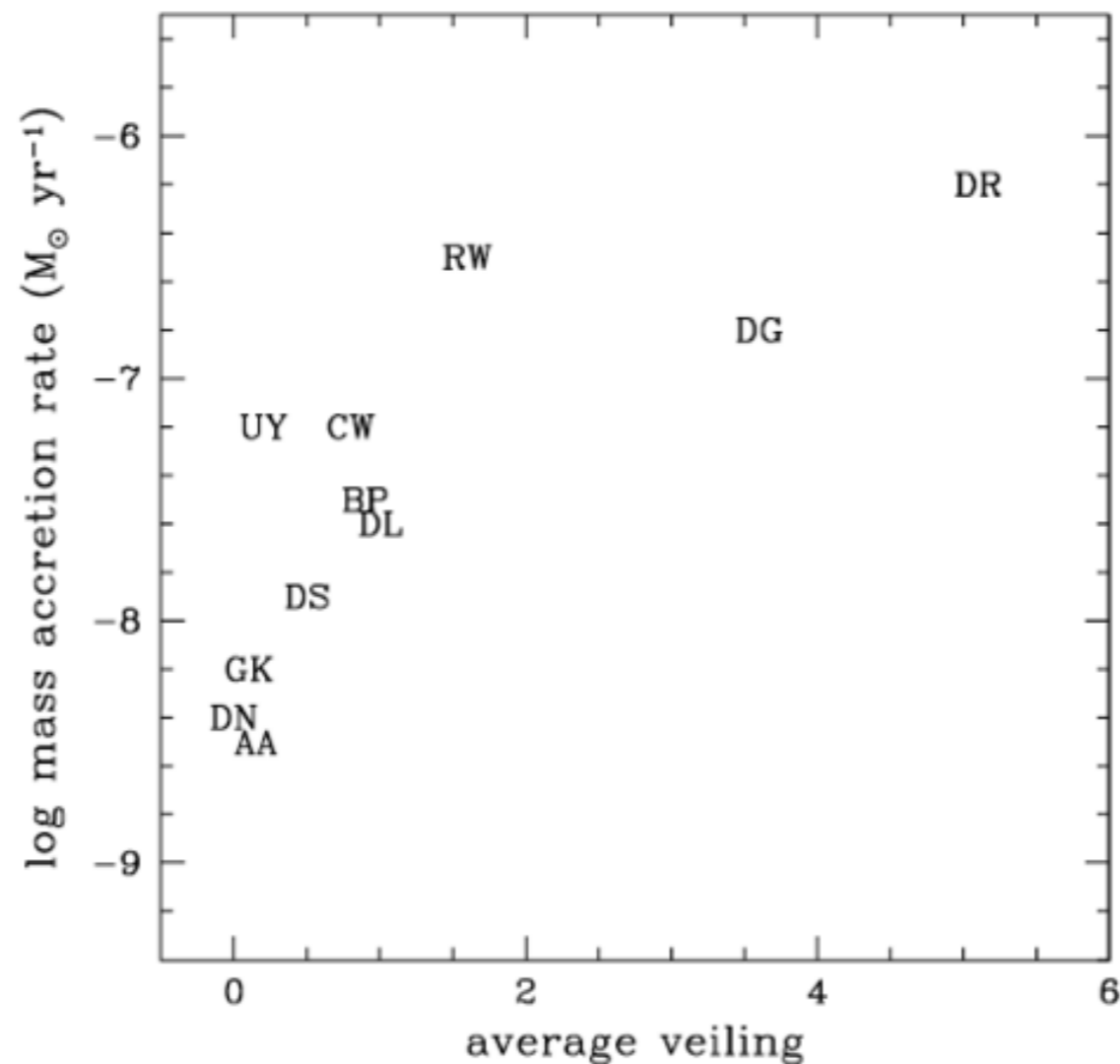


- ❖ Veiling reflects accretion rate! Let's use it instead of veiling...

# Correlations

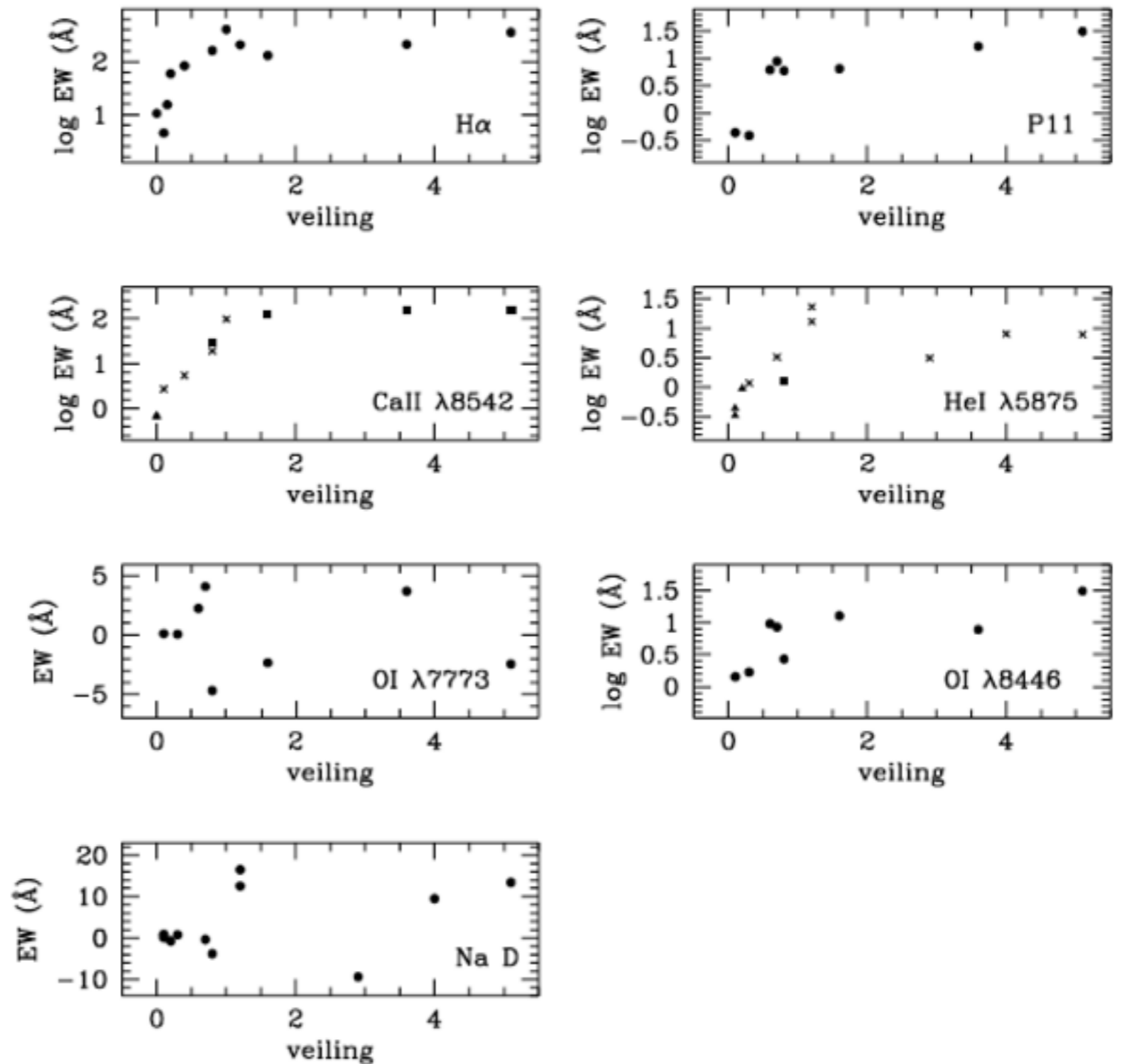
---

- ❖ Average veiling vs. accretion rate
- ❖ well correlated
- ❖ earlier accretion rates are valid for our epoch, too



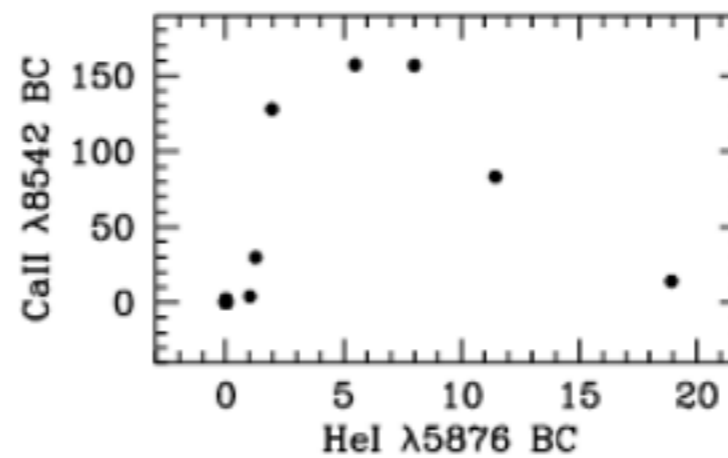
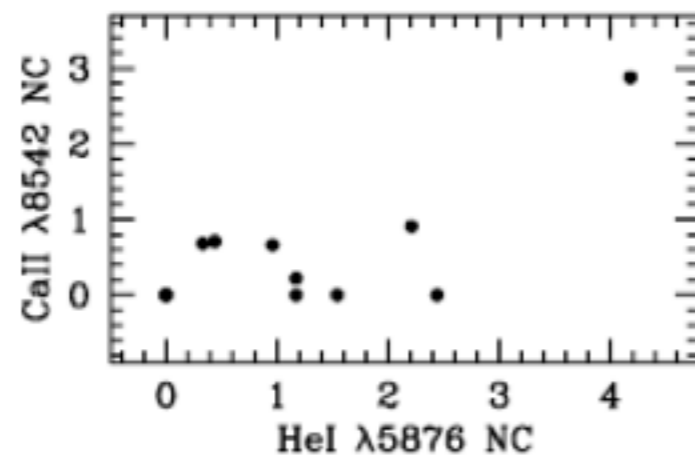
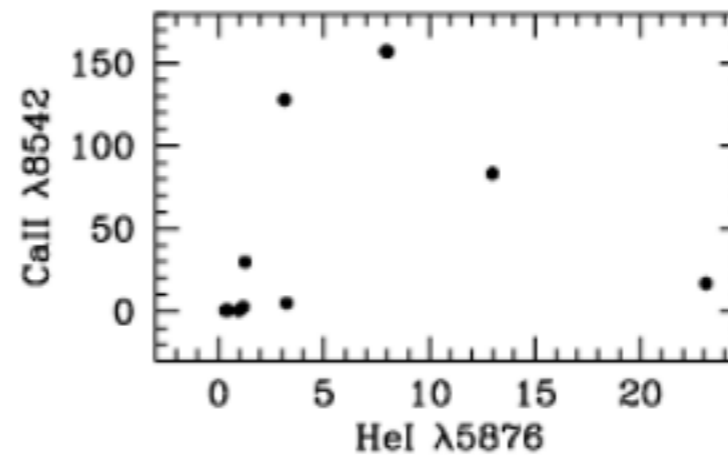
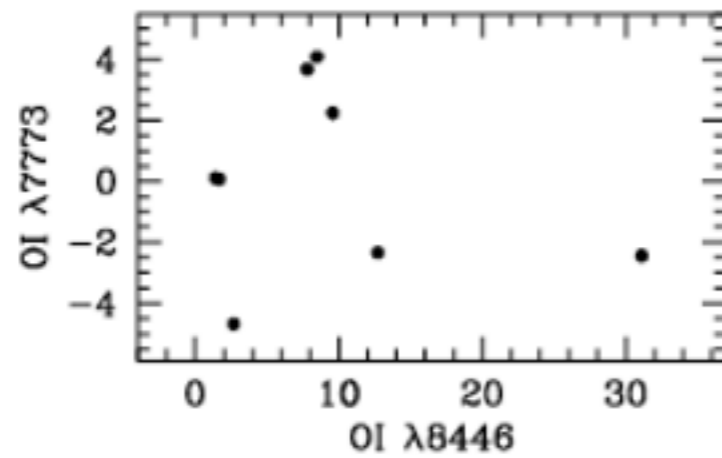
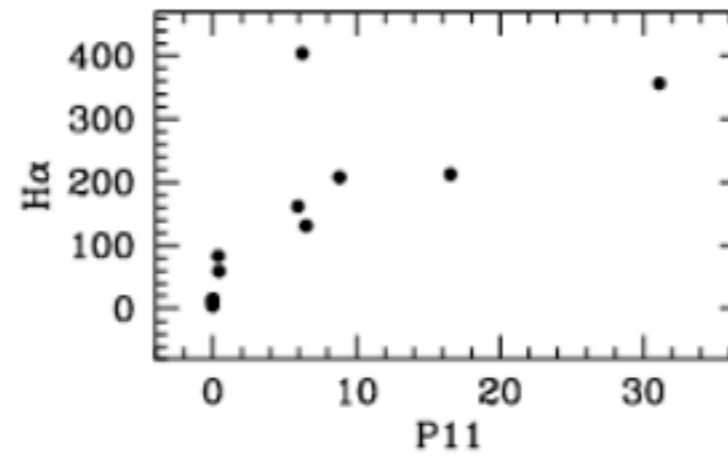
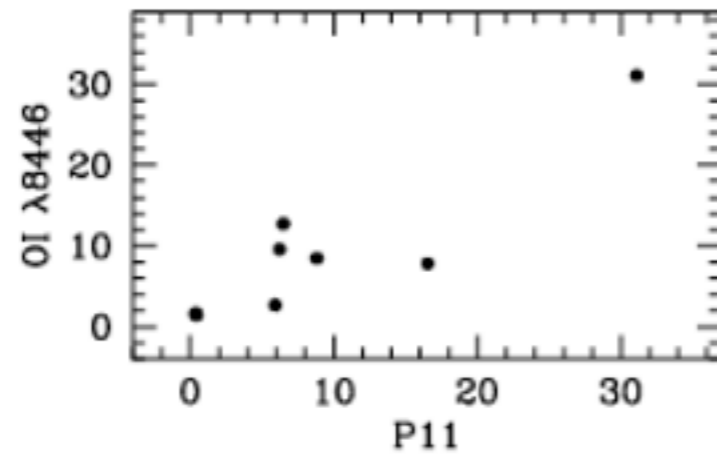
# Emission line equivalent widths

- ❖ EW depends on continuum flux
- ❖ Because of veiling, correction is needed:  
 $W_0/W_r = 1 + r$
- ❖ Trend: increasing EW with increasing veiling
- ❖ Ha, Ca II, and He I seem to saturate (B-type morphology does not correlate with veiling)
- ❖ OI 7773 & Na D does not correlate (contaminated by blue shifted absorption)



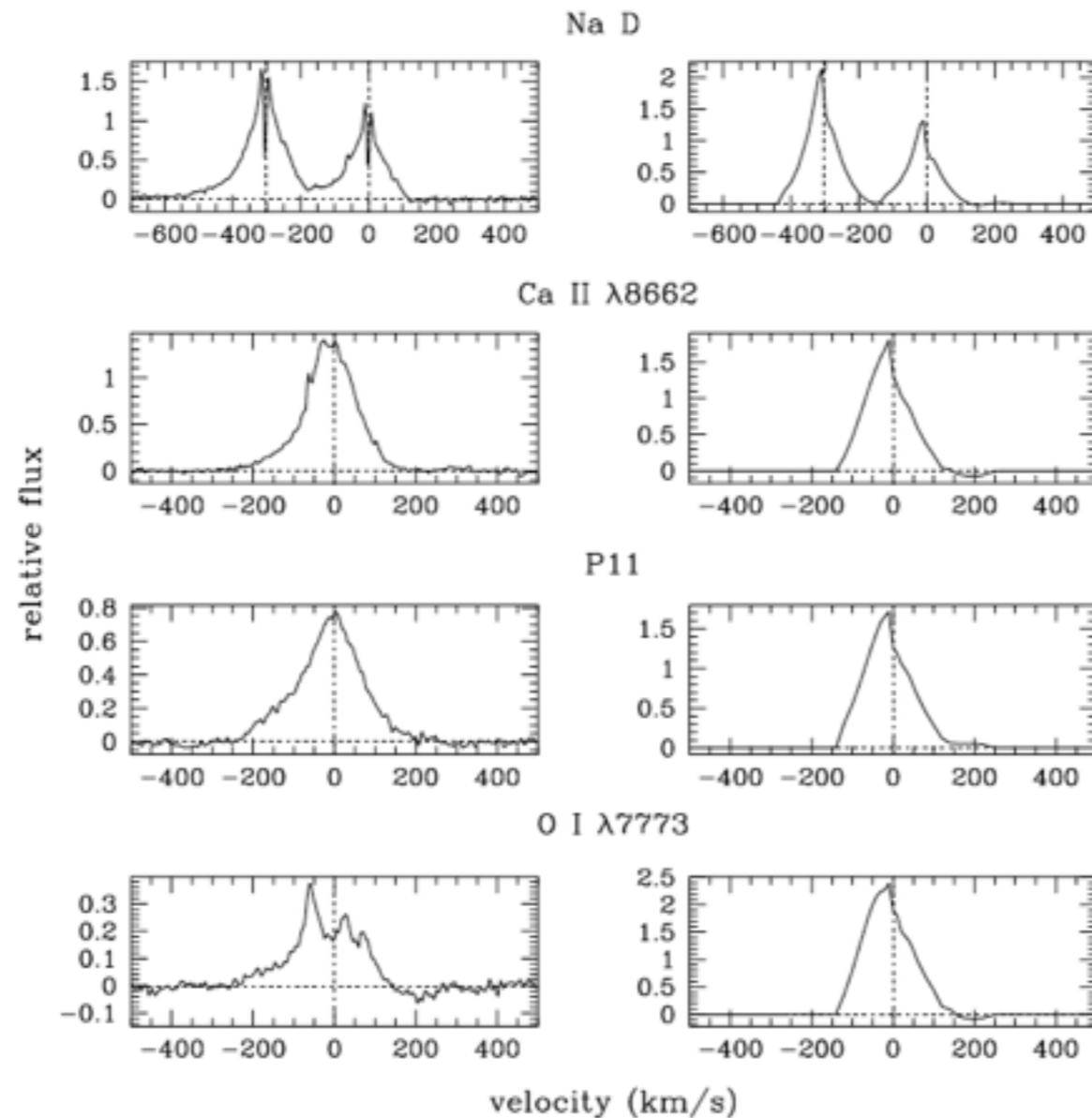


# Emission line equivalent widths



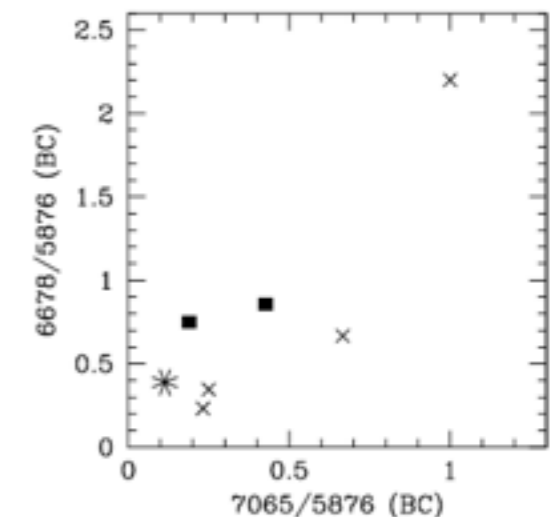
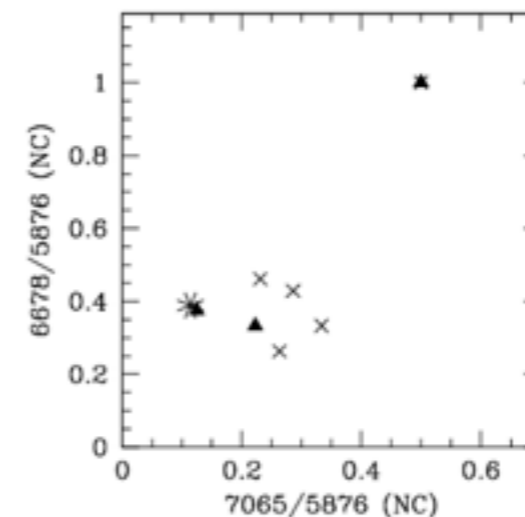
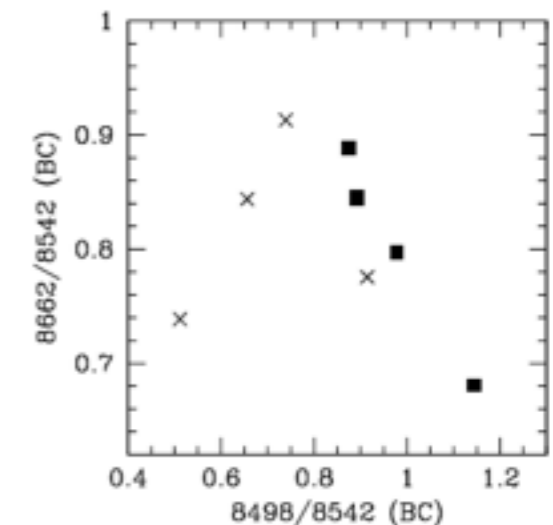
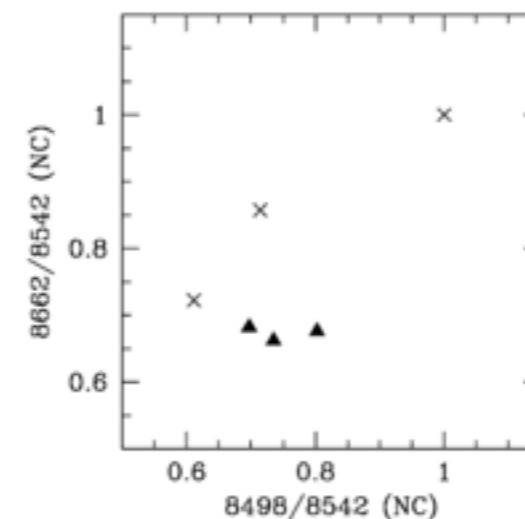
# Line Emission Origin : Magnetospheric Infall ?

- ❖ Broad components are from a common emitting region
- ❖ Muzerolle et al. modeled Balmer lines arising from infall
- ❖ Direct comparison for BP Tau for several atoms (8-levels):



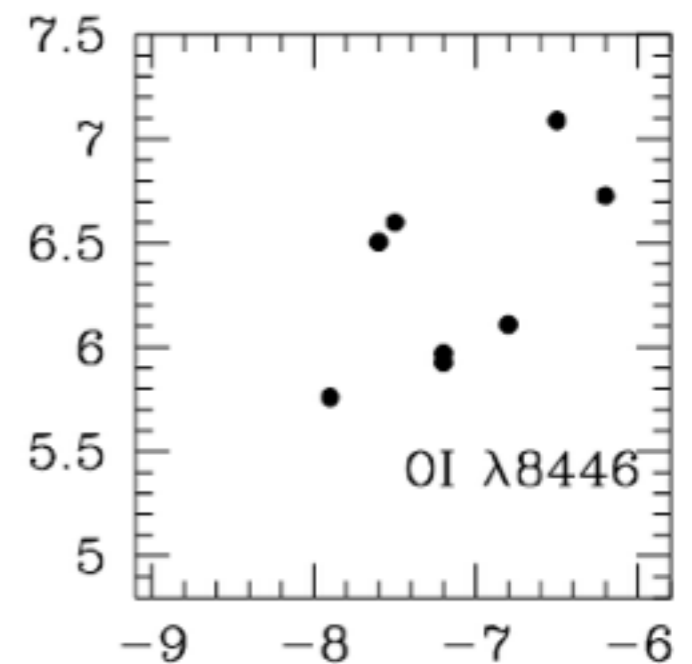
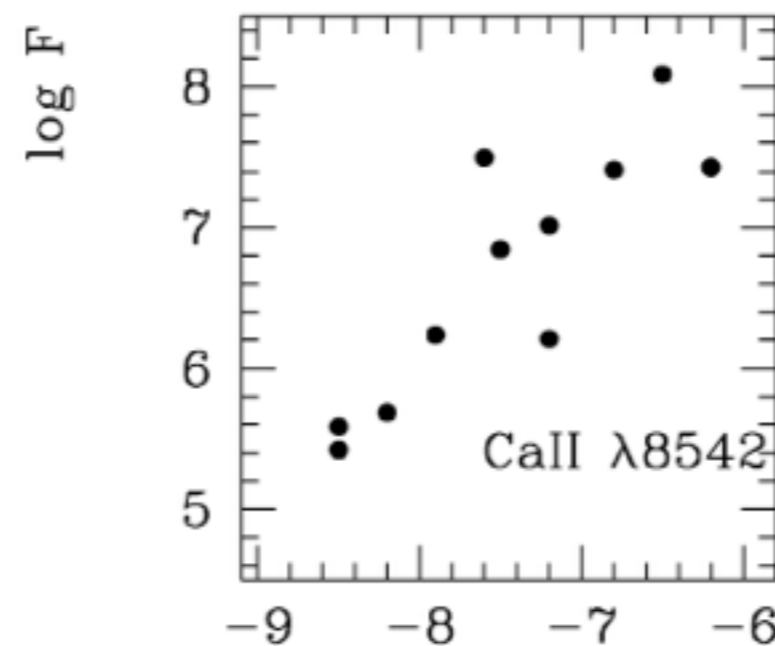
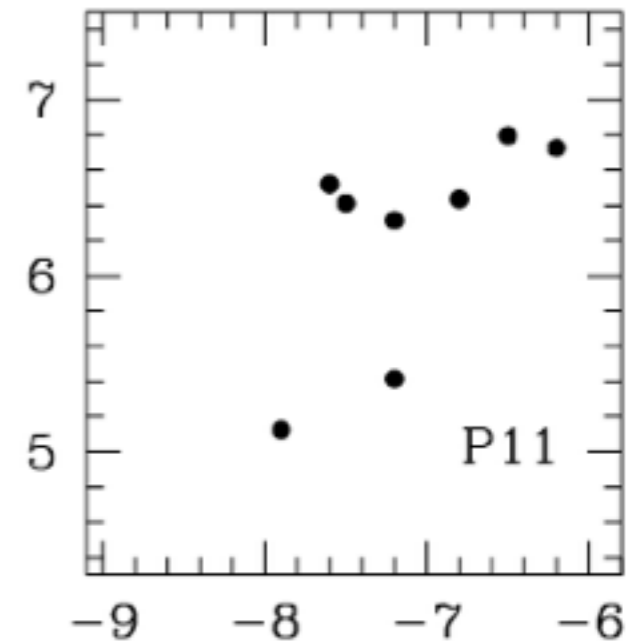
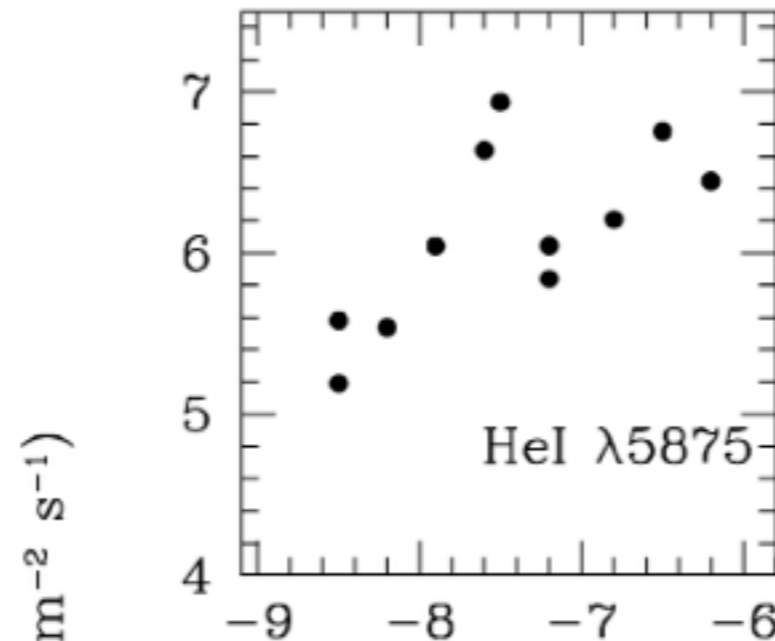
# Magnetospheric accretion diagnostics

- ❖ Goal: how the lines of different atomic species can be used to constrain the physical parameters of the line-emitting region
- ❖ For BP Tau we have a working model
- ❖ Na D is strongly depends on temperature (ionized)
- ❖ It is opposite to hydrogen behaviour
- ❖ Temperature  $\sim 10,000$  K for BP Tau
- ❖ Ratios of the O I lines
- ❖ Line ratios of the Ca II triplet and He I



# Accretion rate indicators

- ❖ A proxy for the hot blue continuum excess
- ❖ Line fluxes (not EW) are used
- ❖ Ca II 8542 AA: strikingly tight correlation.
- ❖ Pa11 and O I 8446 exhibit threshold-like behaviour



$\log \dot{M}$  ( $M_{\odot} \text{ yr}^{-1}$ )